RESEARCH ARTICLE

VOLCANICA

# Lithospheric geotherm and basalt assemblage beneath Nemrut and Suphan volcanoes (East Anatolia): inference from integrated geophysical-petrological modeling

Naeim Mousavi* α,β

α International Institute of Earthquake Engineering and Seismology, Tehran, Iran.
β State Key Laboratory of Lithospheric Evolution, Institute of Geology and Geophysics, Chinese Academy of Sciences, Beijing, China.

## Abstract

Understanding volcanic processes including eruption mechanisms depends on knowledge of temperature and chemical composition (thermochemical structure) of the crust and the upper mantle. This study applies an integrated geophysical-petrological modeling constrained by available seismic information to study the crustal and upper mantle thermochemical heterogeneities in two active volcanoes, Nemrut and Suphan (East Anatolia). The results reveal significant assemblage of basalts at depth beneath Nemrut and Suphan volcanoes. The assemblage of basalt is correlated with considerable lithospheric thinning/disappearance. Predicting geoid height anomaly and fitting gravity data including free-air and Bouguer anomalies supports the presence of the basaltic body as well as the modeled thermochemical structure. This study also implies that the crustal density structure can be biased in the presence of the significant sub-lithospheric heterogeneities. The temperature of the Moho is ~1118 °C, while the temperature of the underlying asthenosphere exceeds 1420 °C, beneath Nemrut and Suphan. The intense seismicity and focal mechanism type (strike-slip and thrust) suggests the magma differentiation and ascent of multiple magma intrusions beneath Nemrut and Suphan, which is supported by asthenospheric and extensional tectonics. Magmatism in East Anatolia is likely to be associated with a low-degree of anhydrous melting of the asthenosphere while hydrous melting is unlikely.

Keywords: Compositional heterogeneities; Thermal structure; Melting model; Seismic data; Potential field; Geoid height; Nemrut and Suphan.

Submitted: 2024-06-29 | Accepted: 2025-07-09 | Published: 2025-11-13

Editor: J. Farquharson | Typesetter: J. Farquharson

## 1 Introduction

Lithospheric mantle-asthenosphere interactions are fundamental in triggering magma ascent. Seismicity can be an indicator of magmatic processes but do not indicate the chemical processes or physical properties of the active magma. Among others, one essential criterion for the characterization of magma evolution and for monitoring of magmas is the temperature of the magma at depth. Another challenge is determination of the composition of the deep-seated material, e.g. in the uppermost mantle and the lower crust, which appears to be the main originating source for erupted magma in the early phases of differentiation. Temperature is often approximated by seismic tomography [Goes et al. 2000; Cammarano et al. 2003; Priestley and McKenzie 2006; Ho et al. 2016; Kumar et al. 2022] and determination of isotherms, e.g. Lithosphere Asthenosphere Boundary (LAB) and/or Curie point depth (580 °C). However, determination of temperature at depth requires careful attention as the information from lower crust and uppermost mantle cannot be directly measured. The chemical composition of magma at depth is estimated using lab analysis of geochemical data from erupted lava which is relatively accurate compared to thermal estimation. Understanding of the nature of magmatism depends on knowledge of lithospheric processes which are characterized by simultaneous thermal and compositional (thermochemical) properties.

Density and seismic velocity are functions of both temperature and composition. Therefore, we can apply geophysical modeling to determine the density and accordingly to quantify the composition and temperature at depth. The modern approach to calculate the density structure takes place through the calculation thermochemical structures within the integrated geophysical-petrological modeling [Fullea et al. 2009]. This approach allows the constraint of density models by geochemical, geophysical, and seismological data. According to McKenzie [1968, 1977], in the absence of mantle flow, the upper mantle thermal heterogeneities explain the density changes which have distorting effects on the measured gravity data. At the same time, density structure plays a crucial role in the calculation of surface topography through consideration of the hydrostatic pressure equilibrium [Molnar et al. 2015].

East Anatolia is known as an active seismic system which is evidenced by recent seismicity. Although seismicity does not necessarily equate to volcanism (it could be simply from the accumulation of strain in the elastic regime), earthquakes can show volume change (non-double couple component in the moment tensor/focal mechanism) which can be used to trace magmatic activity. According to the USGS earthquake catalogue [United States Geological Survey 2024] (Figure 1B), two mega-earthquakes with magnitudes greater than 7 Mw, together with a large number of earthquakes with magnitudes greater than 5 (Mw, Mb, and Ms), have occurred in the vicinity of Nemrut (Nemrut Dagi) and Suphan (Süphan Dağ) volcanoes (Figure 1A). Nemrut and Suphan are composite stratovolcanoes with activity during Pleistocene and Holocene. Suphan volcano is the second highest volcano in Turkey. Nemrut and Suphan have been erupting since 1.0 Ma and 2–0.1 Ma, respectively. The most recent activity of Suphan dates back to

* moosavi.naeim@gmail.com

10 ka in contrast to the recent eruptive activity of Nemrut during the fifteenth and sixteenth centuries (1441, 1597, and 1692 CE) [Yılmaz et al. 1998; Karakhanian et al. 2002; Ulusoy 2008]. In addition to the recent eruptions, analysis of geochemical modeling, volcano seismicity, and gas emissions [Çubukçu 2008; Ulusoy 2008; Ulusoy et al. 2012; Schmincke and Sumita 2014; Ekinci et al. 2020] evidence the ongoing magmatic activities beneath Nemrut and Suphan.

Several problems have remained unsolved with respect to East Anatolia and about the magmatic system under Nemrut and Suphan volcanoes. First, there is no local thermochemical structure of the crust and upper mantle to be used for estimating the density structure in East Anatolia. Second, crustal and upper mantle thermal and compositional heterogeneities under Nemrut and Suphan have not been determined. The temperature of the Moho and the asthenosphere beneath the volcanic system in East Anatolia has not been extensively studied. Third, the available studies on the density structure have been performed focusing on crustal heterogeneities in the absence of the deep thermochemical inference of the density. This leads to biased estimates of the density values which are influenced by distribution of the entire mass from the surface down to, in theory, the core. Fourth, the relation between deep volcano seismicity, crustal heterogeneities, and lithospheric processes in East Anatolia, in particular under Nemrut and Suphan volcanoes, is unknown. Finally, most density models based on fitting gravity data ignore asthenosphere heterogeneities. It has not been quantified how important this simplification could be in determination of crustal heterogeneities.

This study aims to provide a model of the crust and upper mantle thermal and compositional (thermochemical) heterogeneities beneath East Anatolia with a focus on Nemrut and Suphan volcanic systems. A comprehensive set of seismic data (receiver function, tomography, and velocity profiles) is applied to image the crust and upper mantle initial structure (the depth to intra-crustal layers, Moho depth, and LAB depth) and temperature. The composition is constrained based on local and global geochemical data. Integrated geophysical-petrological modeling allows consideration of thermal heterogeneities in the sub-lithosphere [Fullea et al. 2015; Mousavi et al. 2023b]. In light of the presentation of this constrained thermochemical structure, the physical properties of the model including density and velocity are revealed. The asthenosphere heterogeneity is validated based on seismic velocity profiles and prediction of the observed geoid anomaly and gravity data. The obtained model for heterogeneities is discussed in terms of volcano seismicity and lithospheric processes related to magmatism.

### 1.1 Geological background

GPS velocity vectors illustrate the westward escaping tectonic regime in West Anatolia, while the East Anatolian plate is moving northward [Reilinger et al. 2010]. The study profile is located where the direction of the plate motion varies (Figure 1C). Variation of the plate motion directionality is associated with an extensional regime, which is known to be the governing tectonic setting in East Anatolia [Göğüş and Pysklywec 2008; Şengül Uluocak et al. 2021]. To the north of East Anatolia, on the southern boundary of the Eurasian plate, compression tectonics formed the Caucasus ranges (Figure 1A). The Izmir-Ankara-Erzincan-Sevan-Akera suture (IAESA) divides the Caucasus ranges from East Anatolia. A better understanding of tectonic activities in East Anatolia requires a deep insight into the seismic tomography. Additionally, qualitative knowledge of upper mantle temperature comes from seismic tomography. In general, fast anomalies are interpreted as cold and warm zones are interpreted from slow anomalies.

The tectonics of East Anatolia are characterized by transition from subduction to continental collision. The former is explained by the detached or partially fragmented slab of the Neotethys oceanic slab or the delaminated lithosphere [Pearce et al. 1990; Lei and Zhao 2007; Bartol and Govers 2014; Skobeltsyn et al. 2014; Portner et al. 2018; Kounoudis et al. 2020]. The age of termination of subduction and transition to delamination and post-collision is approximated between ~10 Ma [Keskin et al. 1998] and ~13 Ma [Rabayrol et al. 2019]. The tearing in slab or removal of lithosphere triggers asthenosphere upwelling which has caused the vast ongoing magmatism (Late Miocene-Quaternary) in East Anatolia. The presence of slow/warm anomalies is demonstrated by tomography models. In particular, very low (<7 $km\,s^{-1}$) Pn anomalies indicate the ultra-thinning and warm geotherm in East Anatolia [e.g. Gök et al. 2003; Al-Damegh et al. 2004; Al-Lazki et al. 2004; Koulakov et al. 2012].

## 2 Methodology

In order to calculate the density and velocity from temperature and chemical composition, this study applies a finite difference technique and a series of equations including: 1) equation of state for material type to solve for the mineral phase equilibria in thermodynamic framework, 2) the coupled equation of pressure and density, and 3) equation of geopotential from density structure. These equations are solved and summarized as part of the integrated geophysical-petrological methodology known as `LitMod3D` [Fullea et al. 2009]. It must be noted that `LitMod` solves the equation of heat transfer for temperature distribution, but this study applies a different approach for calculation of temperature, described in detail in Section 2.1. `LitMod` has been applied for modeling the thermochemical structure of the Iranian plateau and surrounding area [Mousavi et al. 2022; 2023a; b]. This software applies a forward modeling approach where the fit to geophysical observables is achieved by modification of the input parameters (composition, temperature, and geometry) through a trial-and-error process. The modeling approach involves conducting a 2.5D model along a 670-km-long profile in the south–north (S–N) direction in East Anatolia. The selection of this profile is based on the availability of seismic data (seismic data refers to receiver functions, seismic velocity profiles, and seismic tomography.) and geochemical data that enables us to constrain the crustal and lithospheric structure. In practice, a 3D model with a lateral grid step of 3 km along the profile and a vertical resolution of 2 km is constructed. The bottom of the model is at a depth of 400 km as `LitMod` aims to perform modeling in Cartesian coordinates excluding the Earth's curvature. Assuming the bottom of the model at greater depths (>400 km)

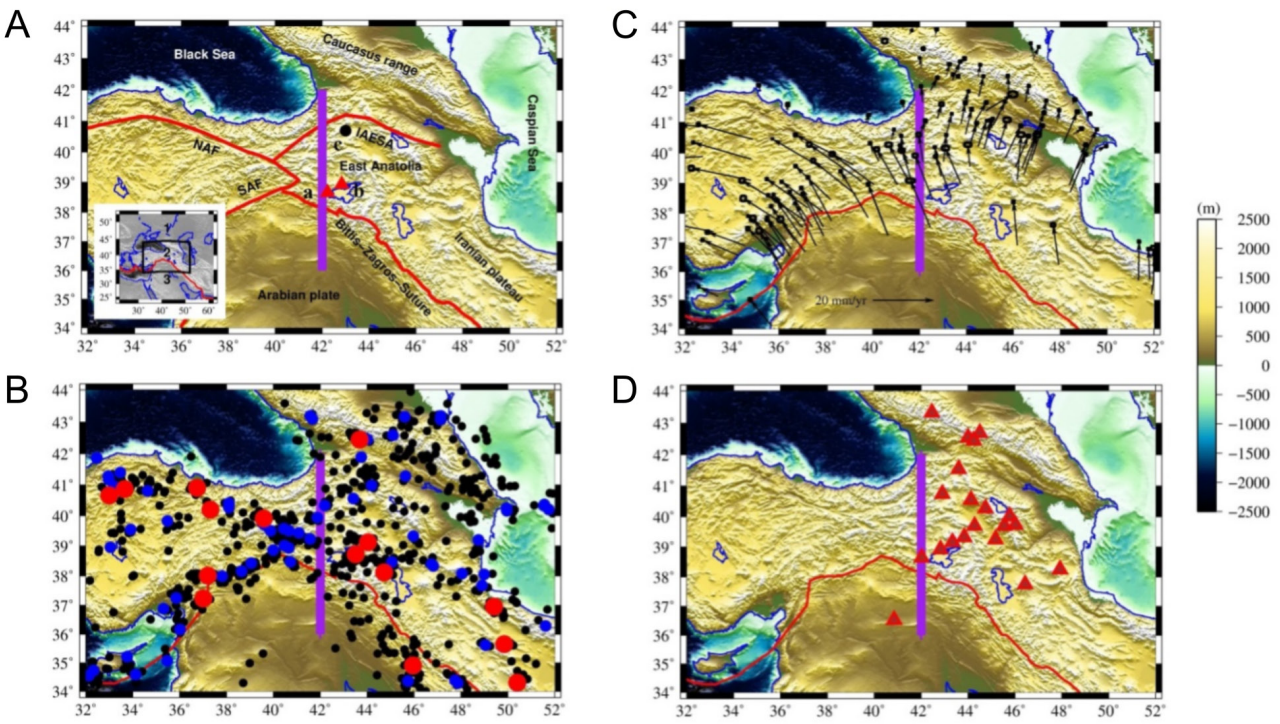


Figure 1: [A] Tectonic domains in the Arabian-Anatolian-Eurasian convergence system. North Anatolian Fault (NAF) and South Anatolian Fault (SAF) are the main active boundaries in the west Anatolia while Izmir-Ankara-Erzincan-Sevan-Akera suture (IAESA) separates East Anatolia from Caucasus ranges in the southern margin of the Eurasian plate. The Bitlis-Zagros Suture zone is at the margin of the Arabian plate collision with Anatolian plate-NW Iranian plateau. The undersea regions are Black Sea (NW) and Caspian Sea (E) surrounding Eastern Anatolia. Numbers in the inset refer to: 1) Eurasian plate, 2) Anatolian plate, and 3) Arabian plate. Letters a to c stand for: a Nemrut volcano, b Suphan volcano, and c Kars plateau. [B] Distribution of earthquake depths from the USGS earthquake catalogue (U.S. Geological Survey, 2024) in Anatolian plate and surrounding. Colored circles present the magnitudes of earthquakes: above 7 Mw (red), between 6 and 7 Mw (blue), and between 5 and 6 with types of Mb, Ms and Mw (black). [C] GPS velocity vectors taken from Reilinger et al. [2010]. [D] Location of volcanoes. Purple line shows the study profile which was chosen based on availability of receiver function, geochemical data, and location of volcanoes.

leads to modeling in larger areas where the modeling must be performed in spherical coordinates to account for the Earth's curvature. In addition, one has to include the effects of olivine to wadsleyite and ringwoodite transitions. The study profile passes through locations of existing geochemical data (Kars Plateau) and crosses Nemrut and the area adjacent to Suphan volcano (Figure 1A). In order to focus on the composition parameter, geometry is taken from seismic studies and kept fixed during modeling. The readers are referred to Section Crustal and upper mantle structure for complete description of the characteristics and quality of the referenced seismic studies.

The value of density and of seismic velocities in the lithospheric, mantle, and asthenosphere is computed as a function of temperature, pressure, and bulk composition (Figure 2). Here, the composition is determined using the major oxide system NCFMAS ($Na_2O$-CaO-FeO-MgO-$Al_2O_3$-$SiO_2$), which is expressed in weight percent (wt.%). Once the major oxides are defined, stable mineral assemblage is calculated by minimization of the Gibbs free energy. The thermodynamic information of all composition types is defined using `Perple_X` software [Connolly 2005]. The stable mineral assemblages in this study are calculated based on the thermodynamic database developed by Holland and Powell [1998]. The stable mineral phase provides the density and velocity in the desired P-T conditions. The bulk density in the model is initially obtained based on phase equilibria and is updated by assumption of lithostatic pressure to include the compression effects by a column of mass above each cell point. Following the creation of the density structure, calculation of the gravity effects and geoid height anomaly is straightforward. The readers are referred to the technical paper by Fullea et al. [2009] for more details about the algorithms and equations for calculation of geopotential fields. In the current version of `LitMod` (version 3.0), density of the crust is calculable based on chemical composition and Gibbs energy minimisation in the crust which allows employing the local constraints for geochemical data [e.g. Keskin 2007].

In this study, the preferred density model is constrained based on fitting the observed gravity anomaly data and geoid height as well as fitting available seismic velocity profiles. In addition, the density structure for the crust is constrained by using geochemical data, while the deep density structure is derived based on tomography-derived thermal structure. Fig-

ure 2 summarizes the workflow of the integrated geophysical-petrological modeling in this study.

### 2.1 Thermal structure

Due to the presence of hot asthenosphere beneath volcanic regions, assuming a steady-state thermal condition seems inappropriate [Mousavi et al. 2023a; b]. Consequently, we cannot solve for a steady-state heat transfer to obtain the upper mantle geotherm in this study. Temperature distribution is taken from tomography following Cammarano et al. [2003] where 0.75 ± 0.15 % variation in ΔVp anomaly corresponds to a temperature change of 100 °C at a depth of 200 km (assuming an adiabatic mantle temperature of 1300 °C). The reference tomography is from Vp perturbation [Koulakov 2011] which has been successfully used to explain sub-lithospheric heterogeneities in the Middle East in previous applications [e.g. Mousavi et al. 2022; 2023b]; in particular in East Anatolia [Şengül Uluocak et al. 2021]. The temperature anomalies obtained from the velocity anomaly by Koulakov [2011] must be converted to absolute temperature.

For calibration of the obtained temperature anomalies, a reference temperature profile is calculated from application of heat transfer equations by `LitMod`. `LitMod` solves for the heat transport based on Drichlet thermal boundary condition (the temperature at surface is 12 °C rising nonlinearly to 1330 °C at LAB depth and reaching to 1520 °C at the bottom of the model following the mantle adiabatic thermal gradient 0.5 °C km$^{-1}$). Solving the heat transfer equation requires assumption of heat production rate in the lithosphere and the values for thermal conductivities for the crust. The crustal thermal conductivity is considered 2 W km$^{-1}$ at the upper layer increasing with depth to the middle crust (2.3 WKm$^{-1}$) and degrades towards the bottom of the crust (2 W km$^{-1}$). The heat production rate is assumed ~1 μWm$^{-3}$ for the crust and 0.01 μWm$^{-3}$ for the lithospheric mantle. The final temperature model is solely based on conversion of seismic velocity anomalies to temperature anomalies and calibration using the reference temperatures for both crust and sub-crustal layer. However, the crustal temperature is mainly inferred from reference temperature as the thermal anomalies in crust are small (up to ~ 50 °C) while they exceed 200 °C in the sub-crustal part. It must be noted that the accuracy of the final temperature profile is validated by comparing the obtained value with the reference seismic studies [e.g. Pesicek and Ryberg 2024].

The derived temperature profile is modified to have the following conditions: the temperature is 12 °C at the surface, is ~1290 °C at the LAB, and the mantle adiabatic thermal gradient is 0.5 °C km$^{-1}$ lead to temperature of 1512 °C at the bottom of the model at depth 400 km. Additionally, the temperature in the model should not exceed ~1527 °C, neither at the bottom of the model nor elsewhere [e.g. Turcotte and Schubert 2002]. The accuracy of the converted absolute temperature is examined by the following tests: 1) the first criterion is that the depth to 1330 °C isotherm in the final temperature structure and the seismic LAB depths from independent studies [e.g. CAM2016 Angus et al. 2006; Koulakov 2011; Ho et al. 2016] representing 1330 °C isotherm must match. If not, the reference thermal profile must be modified, in a trial-and-error procedure, in order to achieve 1330 °C at LAB (summation of temperature change obtained from tomography (e.g. ($\Delta T_{tomography}$ = 40 °C) and the reference temperature profile ($T_{Ref}$ = 1290 °C)). 2) Another criteria is that the final temperature at the bottom of the model must not exceed 1527 °C after addition of tomography-derived thermal anomaly ($\Delta T_{tomography}$ = 15 °C) to the absolute value at the reference temperature profile ($T_{Ref}$ = 1512 °C). Within the lithosphere, temperature in the reference profile is calculated by solving the heat transport equation as a default option for calculating temperature distribution by `LitMod`.

## 3 Data

### 3.1 Crustal and upper mantle structure

The sedimentary cover is taken from Artemieva and Shulgin [2019] which was originally constructed based on Artemieva and Thybo [2013] and Gürbüz and Evans [1991]. The sedimentary cover rises in the central-northern part of the profile in consistency with the receiver functions [Angus et al. 2006] (Figure 3B). The sedimentary thickness is slightly decreased in the Arabian plate. A short length interface appears to depict the upper-lower crust boundary at ca. 20 km. Also, S-wave receiver functions show the bottom of the lower crust (Moho depth), which is in agreement with receiver functions by Karabulut et al. [2013] and Vanacore et al. [2013]. The estimated Moho depth in this study is shallow in the southern part of the profile (Arabian plate) while increasing toward the north in East Anatolia and again shallowing in the Black Sea. Receiver function analysis indicates the crustal thickness exceeds 45 km towards the north in East Anatolia [Angus et al. 2006; Karabulut et al. 2013; Vanacore et al. 2013; Artemieva and Shulgin 2019].

There is an assemblage of considerably low velocity anomalies at depths ranging 70 to 130 km. According to CAM2016 [Ho et al. 2016], the LAB is located at the average depth of 70 km. It means the warm zone in tomography (Figure 3C) represents the hot asthenosphere. There is an estimation of lithospheric thickness by modeling gravity data [Mahatsente et al. 2018] showing a gradual decrease of lithospheric thickness from 94 km in the south to 66 km in the north. The S-wave receiver function presents important interfaces including LAB depth [Angus et al. 2006]. According to Angus et al. [2006], there are two interfaces at depths between 50 and 75 km which coincides with the bottom of the high velocity zone (lithospheric mantle-asthenosphere boundary) identified by Koulakov [2011] (Figure 3C). According to several tomography models, the presence of a fast seismic anomaly (remnant of Neo-Tethyan slab) located at depths between 250 and 350 km at the center of the profile beneath East Anatolia is obvious [Lei and Zhao 2007; Koulakov 2011; Portner et al. 2018]. The top of the low velocity zone in East Anatolia is located at a depth of ~150 km. Almost all of the abovementioned references highlight the presence of a high velocity zone at depths ranging from 150 to 350 km.

Figure 3A represents a compilation of available surface heat flow estimates [Artemieva and Shulgin 2019; Mousavi and Tatar 2024] and measurements (International Heat Flow Com-

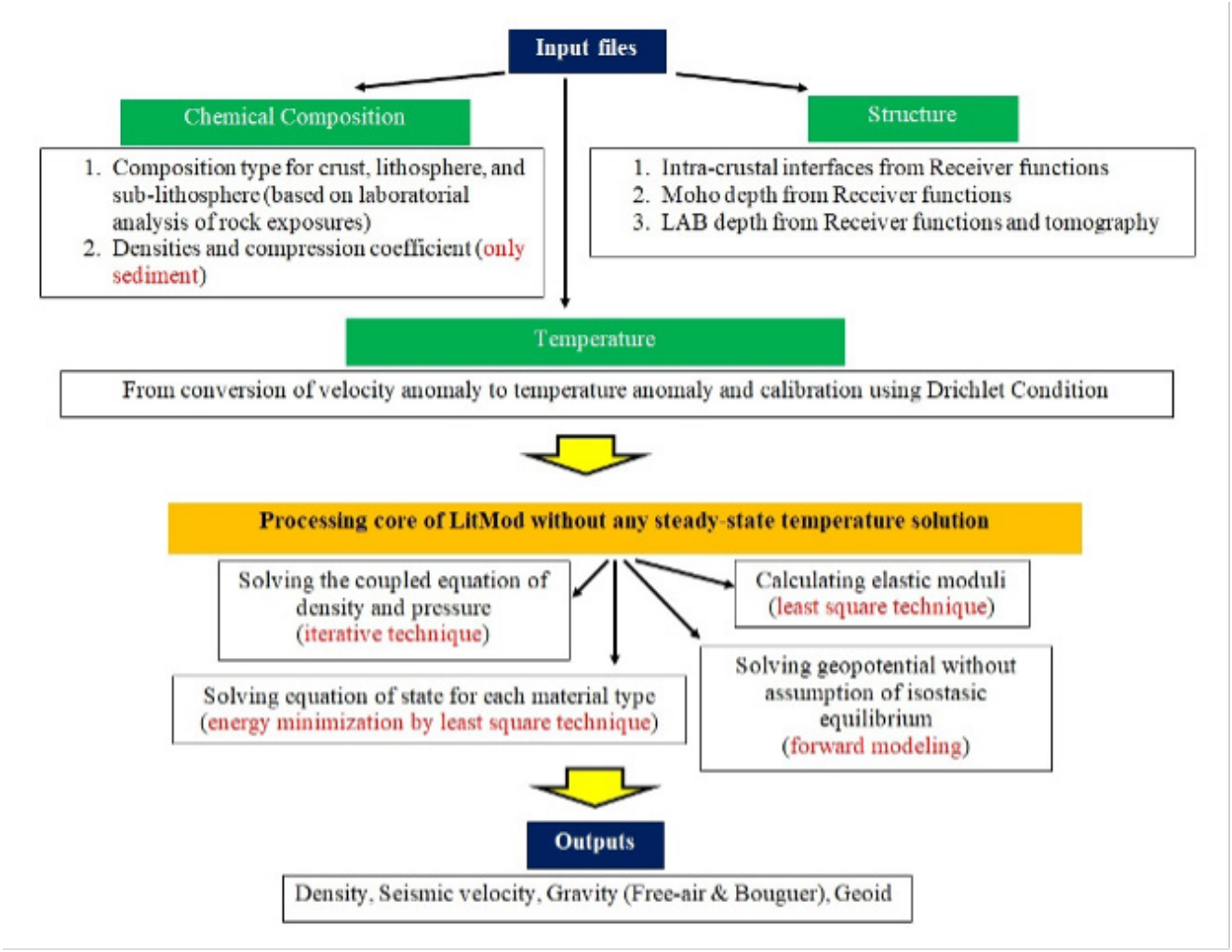


Figure 2: Workflow diagram summarizing the methodology used in this study.

mission) in East Anatolia. The heat flow values are above 60 mW m$^{-2}$ with a maximum of ~90 mW m$^{-2}$ in the vicinity of Nemrut and Suphan volcanoes. The high value of heat flow is associated with lithospheric thinning in East Anatolia indicating a regional high lithospheric temperature.

Presence of mantle density heterogeneities, either high velocity zones at asthenosphere or slow/warm velocity zones, can be associated with residual topography. The surface uplift has partially compensated the crustal root in East Anatolia, but the calculated residual topography of −1.5 to −1.7 km highlights further density heterogeneity within the mantle [Memiş et al. 2020; Şengül Uluocak et al. 2021]. Mahatsente et al. [2018] suggested dynamic supports for −1.7 km residual topography in East Anatolia. They added that the observed high heat flow in East Anatolia is related to upward asthenosphere flow triggered by lithospheric delamination and slab break-off.

### 3.2 Crustal and upper mantle composition

Crustal composition is defined based on XRF analysis of the major oxides from local samples. An average of 5 samples of basaltic rocks [Pearce et al. 1990] represents the basalt composition in East Anatolia (Table 1). The average composition for basalt is depleted (by partial melting) in MgO (5.5 wt.%), indicating the high degree of . Accordingly, in the presence of low MgO and high FeO (11.7 wt.%) the Magnesium Number (Mg#) is significantly lower (45.7) compared to average composition for East Anatolia (52.4; Table 1). A general representative composition of the entire crustal composition in East Anatolia can be derived from study by Keskin (2007) where all (nine samples) crustal major oxides from Kars plateau are summarized [Pearce et al. 1990; Buket and Temel 1998; Keskin et al. 1998] (Table 1). It must be noted that the sedimentary cover is not characterized by composition and is defined by user-defined depth-varying density.

Our understanding of the upper mantle composition beneath East Anatolia is limited due to the lack of mantle xenolith samples. Hence, an average Phanerozoic-type garnet peridotite composition (Table 1, [Griffin et al. 2009]) is selected for the young/refertilized lithospheric mantle of East Anatolia. The selected composition is depleted in $Na_2O$ and $Al_2O_3$, while the $SiO_2$ and FeO contents are comparable to that of the primitive upper mantle PUM (Table 1). The primitive upper mantle (PUM, Table 1) represents the sub-lithospheric part of the model [McDonough and Sun 1995].

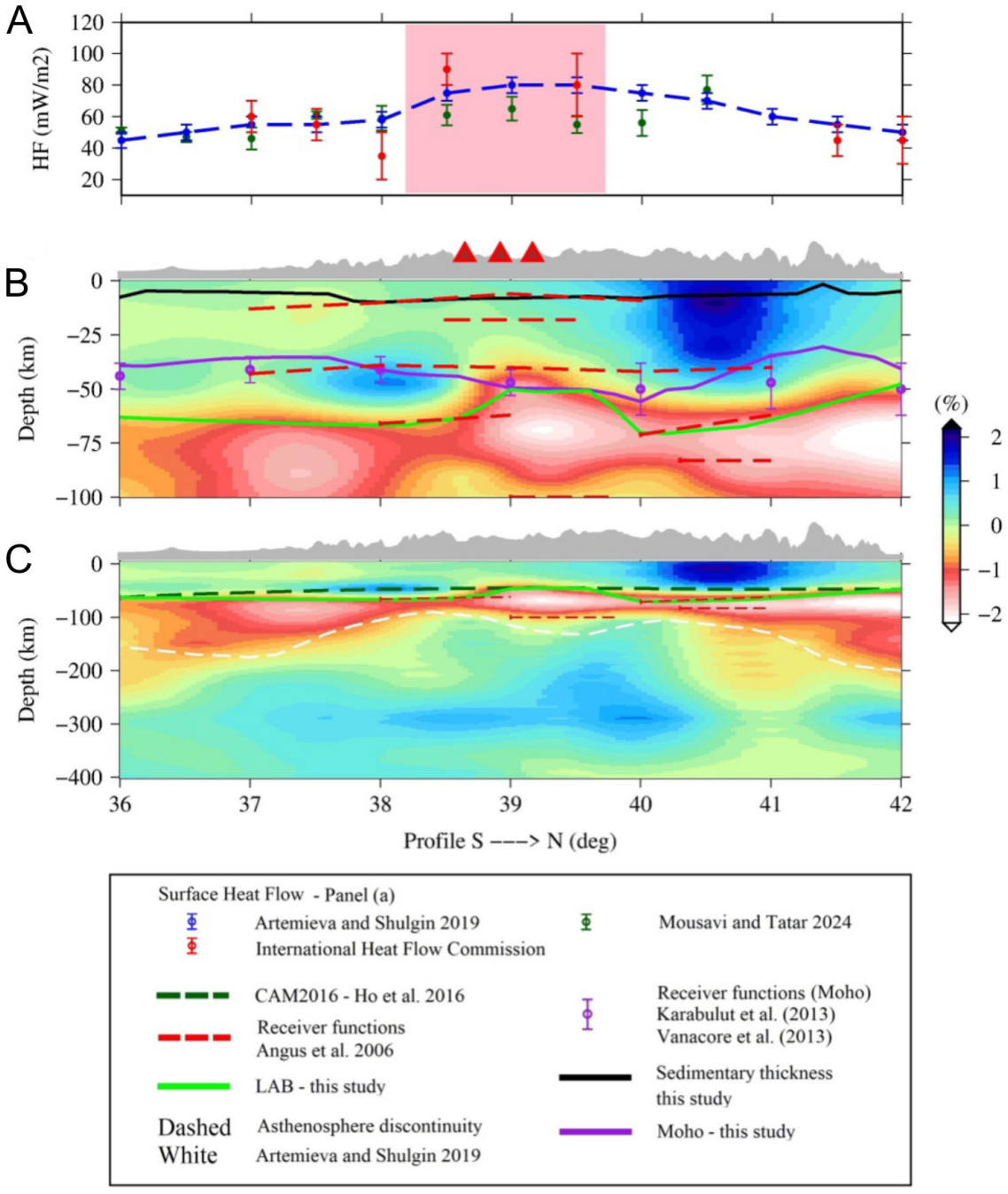


Figure 3: Vp tomography model by Koulakov [2011]. [A] Estimates of surface heat flow by Artemieva and Shulgin [2019] and Mousavi and Tatar [2024], as well as measurements taken from the International Heat Flow Commission. Pink background shows the locality of the volcanic region. [B] A zoomed-in section of the tomography down to 100 km depth. Sedimentary cover, intra-crustal interface, Moho depth, and LAB depth are characterized by S-receiver function [Angus et al. 2006]. Receiver functions by Karabulut et al. [2013] and Vanacore et al. [2013] image the Moho depth. Solid purple line represents the Moho depth in this study. The sedimentary cover is based on Artemieva and Shulgin [2019] and references therein. [C] Tomography down to the depth of 400 km. Green line represents the location of the preferred LAB modified after CAM2016 which is indicated by dashed dark green line. The white dashed line distinguishes the low velocity zone from the remaining asthenosphere approximated after Artemieva and Shulgin [2019]. Figure 1A displays the location of the profile.

### 3.3 Geophysical data

The free-air gravity anomaly and geoid height anomalies are taken from the satellite-based global 2 arc-min (~4 km) Earth model XGM2019, which covers a high degree of resolution up to order and degree 2190 [Zingerle et al. 2020]. Regarding surface topography, this study applies the 1 arc-minute global relief model ETOPO1, developed by Amante [2009], which provides accurate representations of Earth's surface

Table 1: Chemical composition (wt.%) of crust, lithospheric mantle, and asthenosphere from global and local estimates (beneath East Anatolia).

| | Global average for continental crust [Christensen and Mooney 1995] | Local average Kars plateau* [Keskin 2007] | Basalt Kars plateau† [Pearce et al. 1990] | Garnet Peridotite [Griffin et al. 2009] | Asthenosphere** [McDonough and Sun 1995] |
|---|---|---|---|---|---|
| $SiO_2$ | 61.7 | 54 | 48 | 45 | 45 |
| $Al_2O_3$ | 14.7 | 16.5 | 17.1 | 3.9 | 4.5 |
| FeO | 5.1 | 7.8 | 11.7 | 8.1 | 8.1 |
| MgO | 3.1 | 4.8 | 5.5 | 38.7 | 37.8 |
| CaO | 5.7 | 7.9 | 8 | 3.2 | 3.6 |
| $Na_2O$ | 3.6 | 4 | 4 | 0.28 | 0.36 |
| Mg#‡ | 52 | 52.4 | 45.7 | 89.5 | 89.3 |

* Based on nine samples from Pearce et al. [1990], Buket and Temel [1998], Keskin et al. [1998], and Keskin [2007].
† Based on five samples from Pearce et al. [1990].
** Primitive Upper Mantle based on Peridotite, komatiites, and basalts.
‡ Mg# stands for Magnesium number which is defined as Mg# = 100*MgO/(MgO+FeO).

features. Bouguer gravity anomaly is calculated applying a simple Bouguer reduction to the free-air gravity anomaly by XGM2019. Geoid height anomalies are more sensitive to the deep mantle density distribution compared to gravity anomalies because of 1/r versus $1/r^2$ dependence of geoid and gravity anomalies, respectively. Geophysical observables support the modeled temperature, density, composition, and seismic velocity distribution. In the absence of high resolution seismic profiles at deep parts to constrain the density/velocity model, application of geoid anomaly is an important constraining observable. The geoid anomaly is filtered to remove the degrees smaller than 10 from the main signal [e.g. Le Stunff and Ricard 1995], which ensures the sensitivity of geoid anomaly only to the upper mantle above the ~410 km transition zone in East Anatolia. The error of free-air and Bouguer anomalies as well as geoid height is provided by calculating standard deviation of observations at surrounding data points located in one-degree diameter of each data point.

In addition to fitting geophysical observables, in order to validate the obtained density and velocity, two global models of the Earth including PREM [Dziewonski et al. 1981] and AK135 [Kennett et al. 1995] are considered in this study. It must be noted that these models represent a general change of density/velocity within the Earth and the obtained values from this study can deviate from them as they reflect the local features. Therefore, PREM and AK135 are only applied to control the main trend in the calculated density and velocity structures in the upper mantle.

## 4 Results

Model A4 (as the most constrained and preferred model in this study) applies a heterogeneous crustal composition and the sub-crustal thermal heterogeneities based on local geochemical data and tomography, respectively. Alternative models (Model A1–A3) are also conducted to explain the geophysical observables and independent seismic profiles. It must be noted that the interfaces including Moho and LAB depths are based on seismic studies (receiver functions described in section Section 3) and kept fixed during the modeling. First, the effects of asthenosphere thermal structure on geophysical observables (mainly geoid anomaly) and fitting seismic data are examined (Model A1). Model A2 has a tomography-based thermal structure which can explain the sub-crustal seismic structures as well as geoid height anomaly. In order to fit Bouguer and free-air gravity anomaly, crustal composition based on geochemical data is subject to modification (Models A3). A complete description of Models A1–A4 and the reasons for the choice of input parameters is provided in the discussion section.

Figure 4 presents the modeled temperature and density structure in the preferred model (Model A4, Section 5 section) for East Anatolia. The preferred model is able to explain the observed free-air gravity, Bouguer gravity anomalies and the geoid height anomaly (Table 2; Figure 4). Thus, it appears that the density structure in the crustal and lithospheric parts as well as the upper mantle is appropriately defined. The preferred model suggests the presence of a basaltic layer at the lower crust beneath volcanic regions and deeper in the north. The assemblage of basalt is correlated with the lithospheric thinning and location of Nemrut and Suphan. The density of sedimentary cover is on average 2450 $kg\,m^{-3}$, the average crustal density is ~2900 $kg\,m^{-3}$, and the average density of the basalt layer is ~3160 $kg\,m^{-3}$ beneath East Anatolia. As shown in Figure 4, the density change in the asthenosphere is reversely proportional to temperature variations. This implies that the thermal heterogeneities derived from tomography control the density and velocity structure in the sub-lithospheric part. Fitting geoid height anomaly which is sensitive to deep density structure as well as predicting seismic profiles (e.g. Vp from Koulakov [2011]) ensures the appropriate density structure and correct choice of thermal structure.

### 4.1 Crustal physical properties

Thermal structure and physical properties (density and seismic velocity) of crust and lithospheric mantle beneath Nemrut and Suphan volcanoes is presented in Figure 5. Both volcanoes are characterized with a similar geotherm except the temperature under Suphan is a little higher. The thermal structure

Table 2: Statistics of Models A1–A4 including the quality of fit to free-air gravity data, Bouguer anomaly, and geoid anomaly. Misfits are modeled data minus the observed ones. Std stands for standard deviation.

| Model name | Model A1 | | Model A2 | | Model A3 | | Model A4 (Preferred Model) | |
|---|---|---|---|---|---|---|---|---|
| Crustal composition | Homogeneous (Global) | | Homogeneous (Global) | | Homogeneous (Local) | | Heterogeneous* | |
| Upper mantle composition** | Phanerozoic Peridotite (Lithospheric mantle) and PUM | | | | | | | |
| Sub-lithospheric heterogeneities | No | | Yes | | Yes | | Yes | |
| Sediment density ($kg\,m^{-3}$) | $\rho = (1 + \alpha z)^{\dagger}$ | | | | | | | |
| | Mean | Std | Mean | Std | Mean | Std | Mean | Std |
| FA (mGal) | 62 | 39 | 60 | 29 | 55 | 28 | 18 | 16 |
| Bouguer (mGal) | 59 | 39 | 61 | 28 | 56 | 28 | 15 | 16 |
| Geoid (m) | 7.6 | 4.3 | 4.7 | 3.1 | 4.2 | 2.7 | 0.7 | 0.5 |

* Heterogeneous composition is based on the average local and addition of basalt described in Table 1.

** Lithospheric mantle composition and sub-lithospheric composition are described in Table 1, respectively.

† $\rho_0$ = 2450 $kg\,m^{-3}$ is the initial density for sediments, $z$ is the depth, and $\alpha$ is the compression coefficient set to 0.001. The density increases to 2700 $kg\,m^{-3}$ at the bottom of the sedimentary cover.

in the crust is consistent with previous study on lithospheric geotherm of East Anatolia [Artemieva and Shulgin 2019]. On top of the asthenosphere (depths 60–80 km), the temperature exceeds the solidus temperature [Katz et al. 2003]. In the next section, the possibility of melting under East Anatolia is further explored. The calculated Vp velocity is in agreement with an average velocity for volcanic regions [Pesicek and Ryberg 2024]. Similarly, the obtained density in this study is in agreement with the velocity-to-density conversion made using an empirical relation by [Mousavi et al. 2022]. The Vs velocity varies between 3.75 to 4 $km\,s^{-1}$ in crust under Nemrut and Suphan (Figure 5). The crustal composition plays an important role in predicting average velocity value for volcanoes [Pesicek and Ryberg 2024] as using an average composition for continental crust [Christensen and Mooney 1995, Table 1] leads to smaller velocity values than expected (~6.5 versus ~7 $km\,s^{-1}$).

### 4.2 Sub-crustal density, velocity and melting

In the sub-lithospheric part, the resulting density and velocity structure are in general agreement with global models PREM and AK135. The obtained model is additionally constrained based on Vs velocity model CAM2016 [Ho et al. 2016]. In addition, the predicted Vp derived from tomography-based geotherm [Koulakov 2011] can explain the lithospheric low velocity and asthenosphere high velocity zones (Figure 6). The geotherm changes along the profile due to sub-crustal heterogeneities like presence of slab and warm upwelling. There is a good agreement between the predictions and reference velocity (Vp and Vs) and density models along the profile. This indicates that the thermal and consequently density distribution in the sub-lithospheric part is appropriate. As the asthenosphere constitutes almost 80 % of the density column (~70 km lithosphere out of 400 km upper mantle column), its density is a crucial parameter in fitting gravity data and geoid anomalies. Figure 6 illustrates that the model without mantle's thermal heterogeneities (neglecting the presence of cold bodies in the asthenosphere) for East Anatolia fails to predict the velocity profiles.

The asthenosphere temperature (depth 71 km) at 380 km distance from the origin of the profile is 1472 °C while the solidus temperature is 1332 °C (dT= +140 °C). Regardless of the melting mechanism (hydrous or anhydrous), the melt inclusion affects the seismic velocity. The expected velocity change due to presence of melt is $\Delta VP = -1.9F$ and $\Delta VS = -2.4F$ where $F$ is melt fraction [e.g. Clark and Lesher 2017]. Figure 6 shows that the predicted velocity does not deviate considerably (< 0.2 $km\,s^{-1}$) from references: CAM2016 [Ho et al. 2016] and Vp [Koulakov 2011], while presence of melt causes significant reduction of the calculated velocity. In the absence of significant low velocity in the reference seismic profiles, extensive anhydrous melting is unlikely.

Kaislaniemi et al. [2014] suggested that at least 200 ppm water is required to form a noticeable volcanic layer from asthenosphere melting even for long durations of magmatism (> 40 Myr). One possible way to introduce melt in the `Perple_X` is inclusion of water in the material [Connolly 2005]. For instance, presence of 22 % melt in the harzburgite is accompanied by 0.64 wt.% water [Shaw et al. 2018] which leads to significant velocity and density reduction in 1200 °C using `Perple_X` [Mousavi et al. 2023b]. Assuming only 100 ppm (0.01 wt.%) water in the asthenosphere has limited effects on density and velocity. Thus, hydrous melting is unlikely in the presence of only ~100 ppm water in the asthenosphere beneath East Anatolia.

Quantifying the exact amount of melt is outside the scope of this upper mantle-scale study which requires high resolution velocity profiles and consideration of many more experiments on young rock samples. It must be noted that the presence of melt reduces the density which can be observed by gravity observations. Currently, the density model suggests a very dense crust and that the lithospheric mantle is highly fertile and anhydrous to compensate for the mass deficiency due to asthenosphere thermal heterogeneities. Therefore, while we expect low density for molten regions, only a low-degree of anhydrous melting might presently occur under Nemrut and Suphan. Further studies are required to quantify the exact amount of melt using high resolution seismic velocity profil-

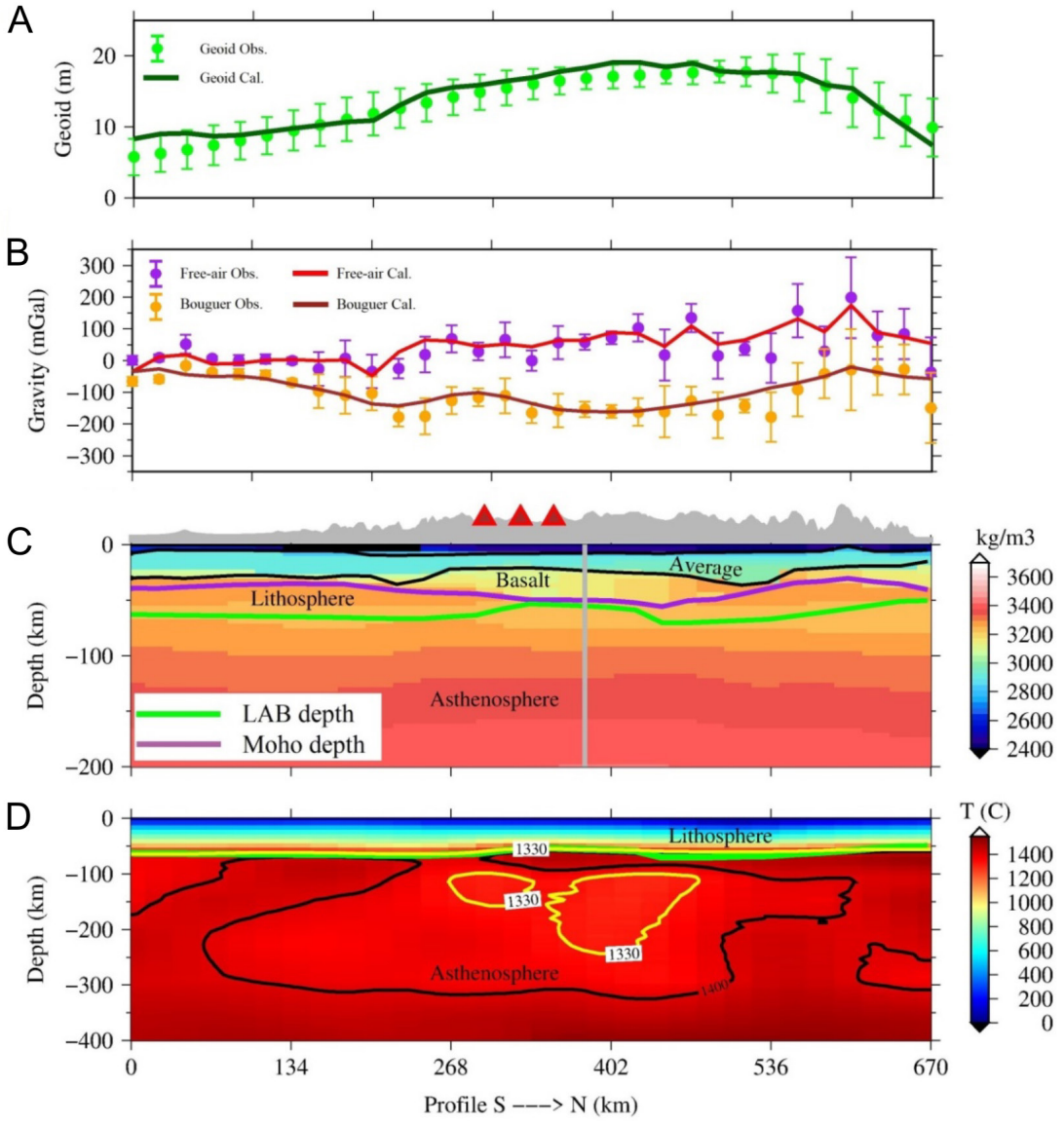


Figure 4: Fitting geophysical observables including geoid [A], and free-air gravity and Bouguer gravity anomaly [B] by the preferred model. Cross sections of the preferred model showing calculated density [C] and temperature [D], which is derived from topography by Koulakov [2011]. Light green line in density and temperature cross sections represents the LAB depth from CAM2016 and was modified using receiver function and considering the bottom of the low velocity zone in the reference tomography by Koulakov [2011]. The figure shows the consistency between the 1330 °C isotherm (yellow line) and seismic LAB (light green). Grey vertical line is the location of vertical profiles shown in Figure 5 and 6 which is selected based on the location of lithospheric thinning.

ing, temperature profiles, or experiments on the hydration of crustal and lithospheric rocks.

The density profiles shown in Figure 7 are the relative density variations at representative distances from the origin (200, 300, etc) which are calculated by division of density values by values from the reference density profile at 100 km distance from the origin of the profile. Figure 7 presents the density variation due to sub-lithospheric thermal heterogeneities along the cross section. The warm zones are interpreted as density deficiencies and the density excess is related to decrease of the temperature. The density excess is limited to ~5 $kg\,m^{-3}$ due to the transition from average to cold zone in the presence of slab remnant, meaning the slab is heated and there is no significant thermal contrast suggested by tomography. The significant reduction of density up to ~-18 $kg\,m^{-3}$ represents crossing the warm region within the asthenosphere. It must be noted that these values are relative density changes and the absolute density of the asthenosphere is shown in Figure 6.

## 5 Discussion

### 5.1 Gravity and geoid anomaly responses of sub-lithospheric (thermal) and crustal (compositional) heterogeneities: sensitivity tests

Different tests are conducted to elaborate the geophysical effects of crustal and upper mantle heterogeneities along the

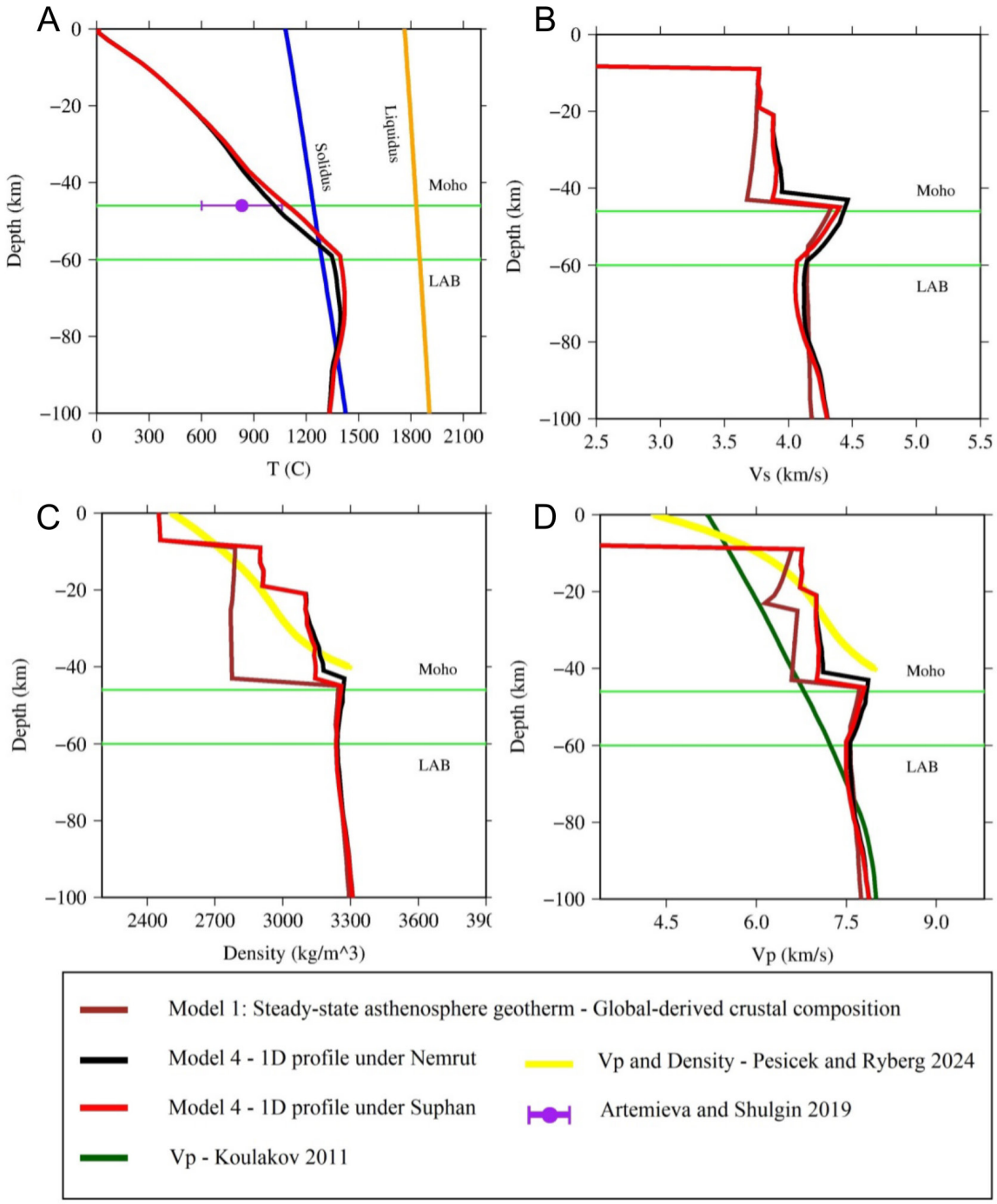


Figure 5: Vertical profiles of crustal temperature [A], Vs velocity [B], density [C], and Vp velocity [D] under Nemrut and Suphan volcanoes.

East Anatolia cross section (Figure 1). The first model (Model A1) aims to assess the geophysical effects of thermal heterogeneities in the upper mantle. This model applies a homogenous geotherm by solving the heat transfer equation assuming steady-state heat transfer and Drichlet thermal boundary condition (see Section Thermal structure for more details). Therefore, there are no lateral or vertical thermal heterogeneities (Figure 8A). Model A1 fails to fit geoid anomalies as well as the observed gravity data indicating the inappropriate temperature and corresponding density structure in the deep part of the cross section (Figure 9). This test indicates the need for thermal heterogeneities within the asthenosphere (Figure 6). The crustal composition in this test is simple and homogenous and taken from global averages [Table 1; Christensen

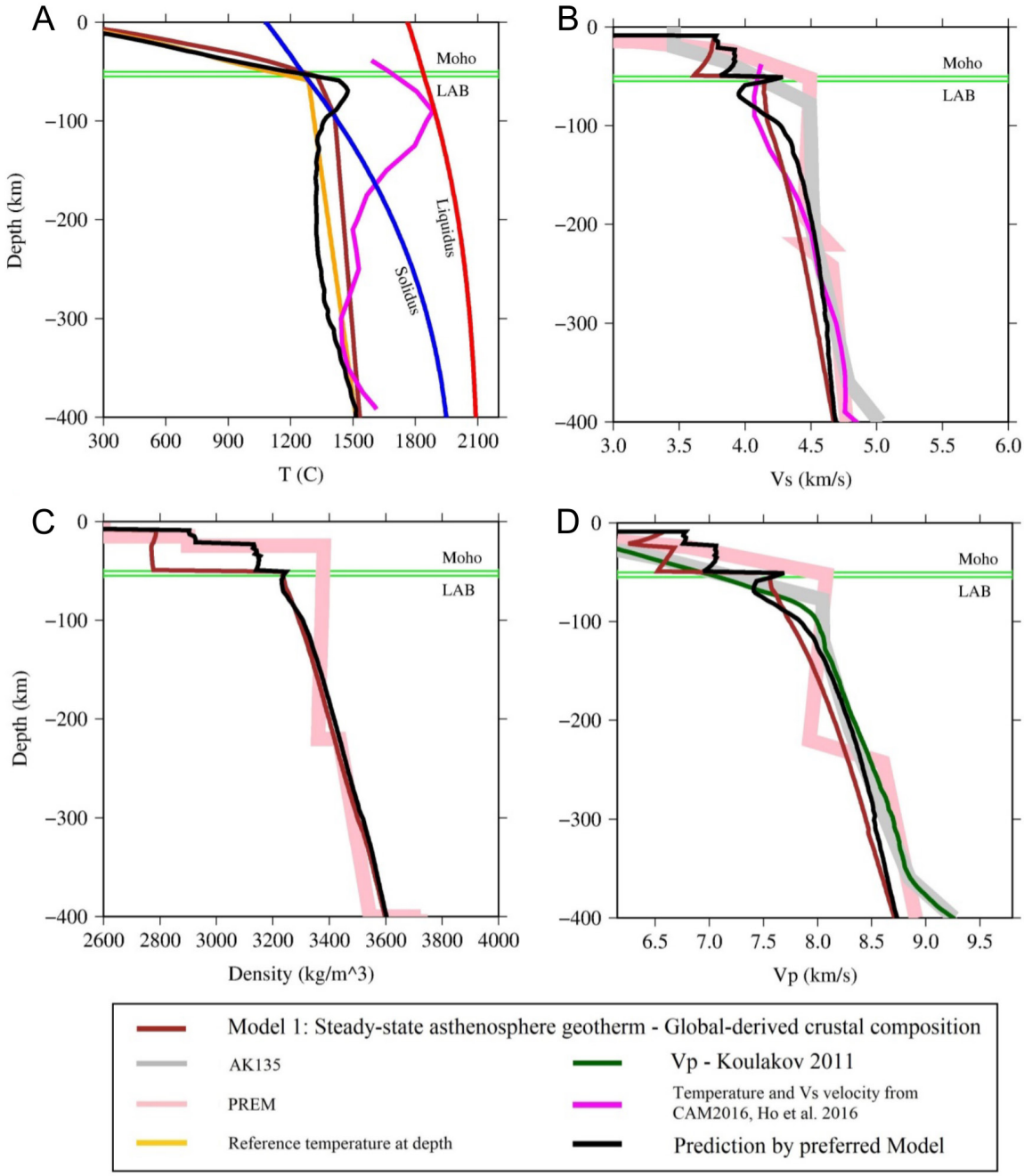


Figure 6: Vertical profiles of subcrustal (lithosphere and asthenosphere) temperature [A], Vs velocity [B], density [C], and Vp velocity [D] at the center of the study profile. The location of profile is shown in Figure 4 as a grey line at 380 km distance from the origin of the profile.

and Mooney 1995] to put emphasis mainly on the thermal structure of the model. It must be noted that the lithosphere is thin and non-existent in some parts beneath East Anatolia; hence the choice of composition for the lithosphere has limited effects on the density model and the fit to geophysical observables. The lithospheric mantle composition is a fertile Phanerozoic type as described in Table 1. The composition of the asthenosphere is set according to the Primitive Upper Mantle PUM (Table 1) in all models.

Model 2 applies the geotherm based on the preferred upper mantle tomography [Koulakov 2011, Figure 8B] and using a homogenous composition for the crust as described in model A1. The fit to geoid and gravity data significantly improves in Model A2, indicating an appropriate thermal and density structure for the asthenosphere (Figure 9A–9C, Table 2). As shown in Figure 6, using tomography-based geotherm in Model A2 provides a better fit to seismic velocity profiles [e.g. Koulakov 2011; Ho et al. 2016] compared to Model A1, which

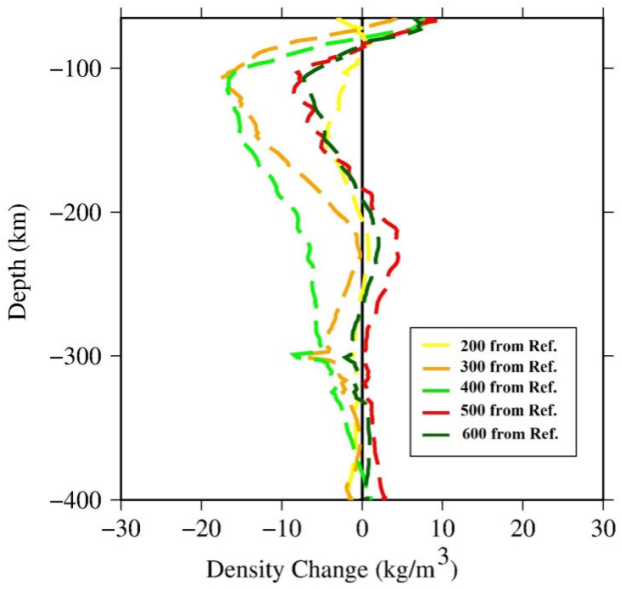


Figure 7: Lateral variation of density along profile due to tomography–based geotherm. Reference density profile is taken from the vertical profile at 100-km distance from the origin, and each relative density profile at different distances from the origin (200, 300, etc.) is calculated by division of the density profile by the reference density profile at 100 km distance from the origin of the profile.

has steady-state thermal structure and homogenous asthenosphere (Figure 8A and 8B).

Model A3 applies the crustal composition based on geochemical data in Kars plateau [Table 1; Keskin 2007] instead of using the average composition from global databases. According to statistics presented in Table 2, application of average composition from local samples does not lead to significant improvement in fitting geophysical observables (Figure 9). However, it is preferred to use local samples for constraining composition in the crust. A noticeable low in the calculated gravity data in Models A2–A3 highlights the lack of mass in the central part of the crust (Figure 9). Model A4 (the preferred model) includes a basalt composition at the lower crust mainly in the central and northern parts of the profile (Figure 3). The intra-crustal interface by receiver function demonstrates the crustal heterogeneity and is applied to define the boundary between the depleted and basalt crustal layers (Figure 3). The composition of basalt is taken from the samples in Kars plateau [Table 1; Pearce et al. 1990]. The best fit to geophysical observables is provided by Model A4 (Table 2). Model A4 also predicts the average velocity (Vp) profile for volcanic regions provided by Pesicek and Ryberg [2024] and estimated crustal density by conversion of the average Vp velocity to density using the empirical conversion method represented by Mousavi et al. [2022] (Figure 5).

### 5.2 Temperature dependence of basalt density

Figure 10 represents the density change of basalt (the composition is defined based on Kars plateau; Table 1) as a function of temperature. In general, the density increases with decreasing temperature with one exception of an extremely warm geotherm with Moho temperature of 1412 °C where the density is not lower than the case of a colder geotherm associated with Moho temperature of 1327 °C. The density change is not linear with depth, and several reductions occur at depths ~15 km, ~25 km, and ~45 km. It seems that there is a pattern for the density drop, as it occurs at shallower depths in warmer geotherms. The deepest density reduction belongs to a test with Moho temperature of 946 °C (blue line at Figure 10). This density reduction in the lower crust (depth ~ 45 km) occurs for the Moho temperature band of ~890—~1075 °C considering that the density is also dependent on the composition of the basalt. The above-mentioned temperature band is very close to the preferred temperature (981 ± 52 °C) at which mafic to intermediate melts reside [Higgins and Caricchi 2023]. In the case of Nemrut and Suphan volcanoes, the Moho temperature is about 1118 °C and the modeled crustal thermal structure and application of basalt composition from Kars plateau (Table 1) does not lead to such reduction in the density profile. However, Mousavi et al. [2023b] observed such a density reduction under the Damavand volcano (supported by Vs velocity profiles) where the Moho temperature is ~1070 °C.

### 5.3 The effects of lithospheric-mantle interactions, geotherm and plate motions on East Anatolia volcanism

Presence of hot asthenosphere beneath the lithosphere of East Anatolia has been qualitatively reported by previous studies [e.g. Keskin et al. 1998; Keskin 2003]. The Vp/Vs in East Anatolia is high indicating the presence of magmatic activity above 100 km depth [e.g. Fichtner et al. 2013; Vanacore et al. 2013; Zhu 2018]. Figure 11A shows the correlation between the slow velocity zone [e.g. Koulakov 2011], high temperature, and the location of volcanism. The dominant explanation for the emplacement of hot asthenosphere beneath lithosphere is the lithospheric delamination or detachment [e.g. Şengör et al. 2003; Lei and Zhao 2007; Göğüş and Pysklywec 2008; Bartol and Govers 2014; Skobeltsyn et al. 2014; Portner et al. 2018; Rabayrol et al. 2019; Reid et al. 2019; Kounoudis et al. 2020]. However, a recent study by Hua et al. [2023] illustrates that the asthenosphere assemblage beneath East Anatolia is fed by the far-field flow originated from the Afar plume. It appears that the mechanism for the assemblage of the hot asthenosphere (Figure 11B) might not be thoroughly understood yet and future studies are required to revisit the impact of the asthenosphere and lithospheric mantle in the production of melts under Nemrut and Suphan volcanoes. Lithosphere-asthenosphere interaction beneath Suphan is well-established [Özdemir and Güleç 2014] while this interaction reaches to the maximum beneath Nemrut [Güleç et al. 2002]. According to Özdemir and Güleç [2014], the contribution of asthenosphere melting in production of Suphan volcanic magma is relatively limited compared to the contribution of the melting degree within the lithospheric mantle during the Miocene-Pliocene.

The high temperature at the bottom of the crust indicates the heating system is fed by the hot underlying asthenosphere. Moho temperature beneath East Anatolia has been approxi-

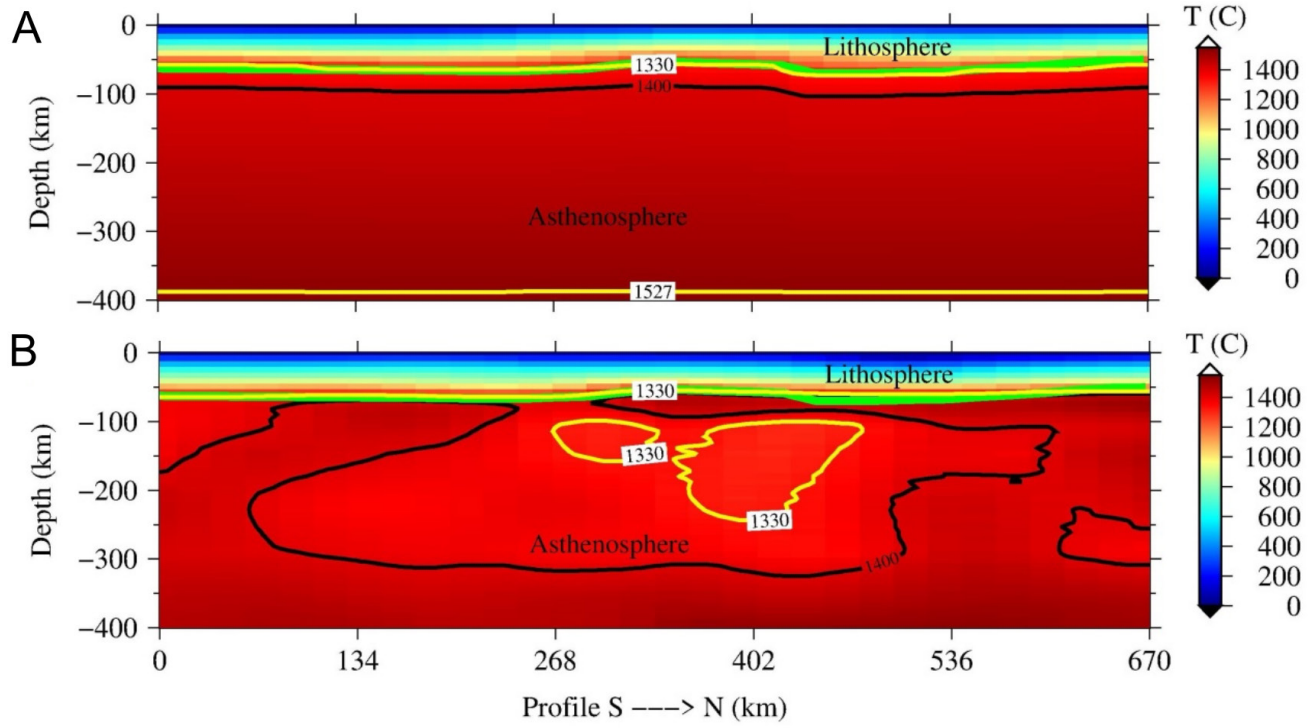


Figure 8: [A] The geotherm is defined based on solving the steady-state heat transfer equation using fixed temperature at surface, LAB, and the bottom of the model. [B] Tomography-based upper mantle geotherm. Green line represents the seismic LAB depth. Yellow contour line is the isotherm of 1330 °C.

mated to be 900 °C [Artemieva and Shulgin 2019]. This Moho temperature is in agreement with the temperature from other young volcanic regions, for example from the western United States, which has Moho temperature greater than >800 °C with an extreme value of 1160 °C [Schutt et al. 2018]. Based on the obtained thermal structure in this study, the temperature of Moho is ~1118 °C, while the temperature of underlying asthenosphere assemblages exceeds 1490 °C, beneath Nemrut and Suphan. According to Çubukçu [2008] the magma reservoir temperature in 4–5 km depth under Nemrut is up to 1050 °C. This means that the temperature of ascending magma slightly decreases while ascending through the crust. Moho and asthenosphere temperatures are between 1070—1130 °C and between 1230—1130 °C in Damavand volcano (North Iran), respectively [Mousavi et al. 2023b].

Geodynamic modeling indicates the synconvergent extension in eastern Anatolia after lithospheric mantle delamination [Göğüş and Pysklywec 2008; Şengül Uluocak et al. 2021]. Considering the direction of plate motions by GPS velocity vectors, the study profile is located at the boundary between northward and westward moving plates (Figure 1C). Different directions for plate motions, which is associated with the extensional regime in East Anatolia, can support the magmatism by lithospheric thinning and asthenosphere suction.

### 5.4 Seismicity and focal mechanisms under Nemrut and Suphan volcanoes

Earthquake hypocenters unveil the activities at depth along the study profile. According to the German volcano monitoring website Volcano Discovery*, since 1900 a total number of 543 and 457 quakes have occurred beneath Süphan Dağ volcano and Nemrut Dagi volcano, respectively. Ulusoy [2008] suggested that the location of the magma chamber beneath Nemrut is around the depth of 4–5 km. Figure 12A represents the location of earthquake hypocenters compared to crustal interfaces (basement and top of the basalt). There is a clear correlation between the location of volcanoes, lithospheric thinning, upwelling of basaltic layers, and the clusters of earthquakes. There are more earthquakes under Nemrut, and the depths of the earthquakes are larger compared to Suphan. Additionally, the earthquakes are continuously spread from the lower crust up to the sedimentary cover. In the study cross section, seismicity under Suphan appears to be limited at great depths. However, the events from the eastern side of the Suphan are absent in this cross section (Figure 12B).

The seismicity noted by USGS is significant (magnitude >5.0), and the Harvard Centroid Moment Tensor catalogue (CMT) Program [Dziewonski et al. 1981; Ekström et al. 2012] provides fault plane solutions (full seismic moment tensor) from which one can calculate the non-double couple components (closest double couple defined from the moment tensor). Most focal mechanisms in East Anatolia are strike-slip with very limited thrust or reverse fault types [Örgülü et al. 2003]. Depiction of CMT plate solutions (1976—2024) under Nemrut presents a concentration of thrust earthquakes that occurred mainly in 2011. Eruptions of Miake-shima, Tori-shima (Japan), and Beerenberg (Jan Mayen Island) volcanoes have

*https://www.volcanodiscovery.com

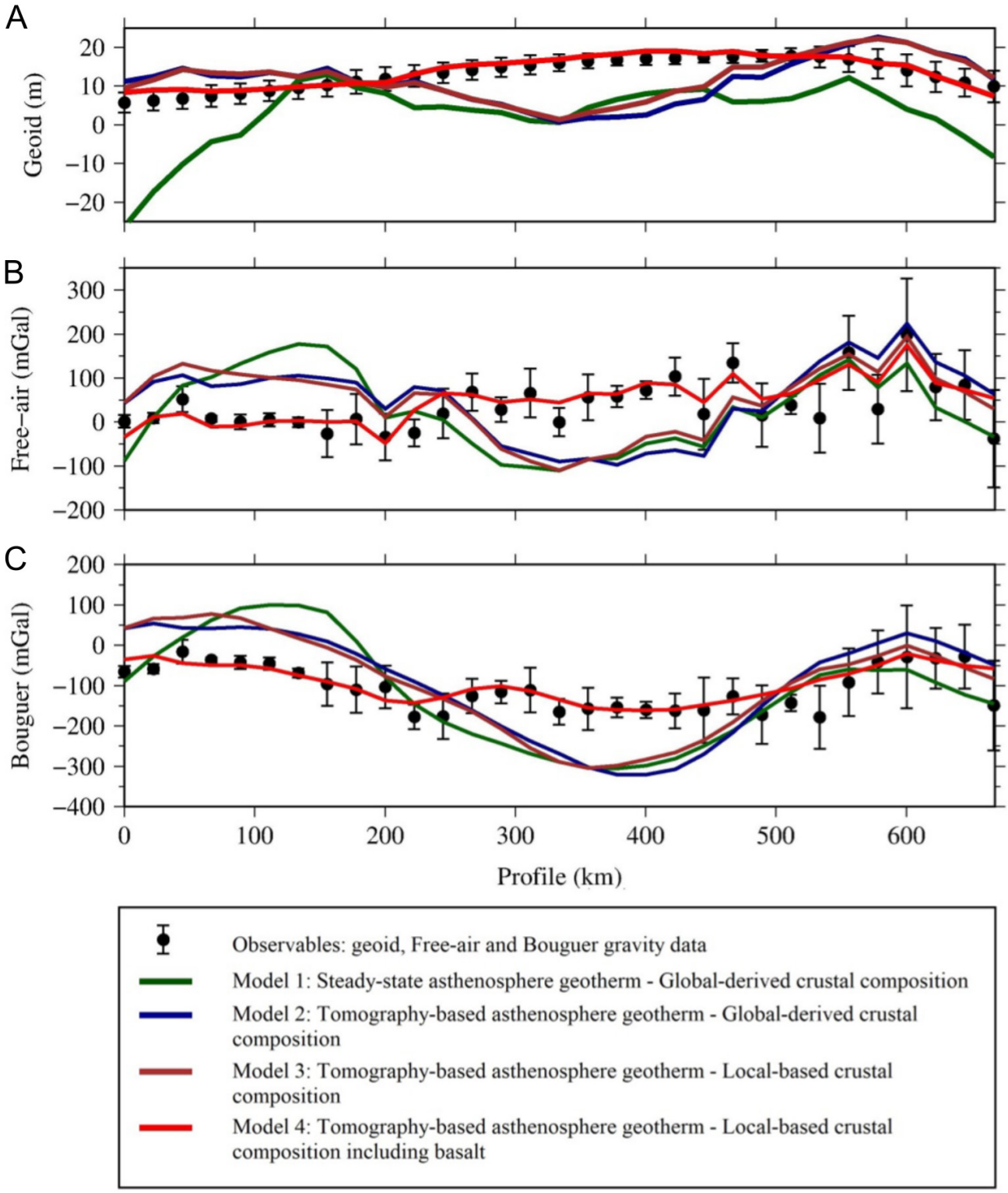


Figure 9: Comparing calculated anomalies geoid [A], Free-air gravity [B], and Bouguer anomaly and observations for Model A1–A4. The composition setting is described in Table 1 while the structure is depicted in Figure 3. The statistics of the modeling procedure are summarized in Table 2.

been associated with the strike-slip earthquakes [Zobin 1972]. Terakawa et al. [2016] also recognized a one-to-one relation between eruption in Mount Ontake volcano and pre-eruption strike-slip and thrust earthquakes, while reverse earthquakes were dominant after eruption. Presence of thrust earthquakes might warn of pre-eruption volcanic activity at Nemrut and Suphan. These thrust earthquakes might be associated with the activity of Bitlis-Zagros main fault. Even in the case of no

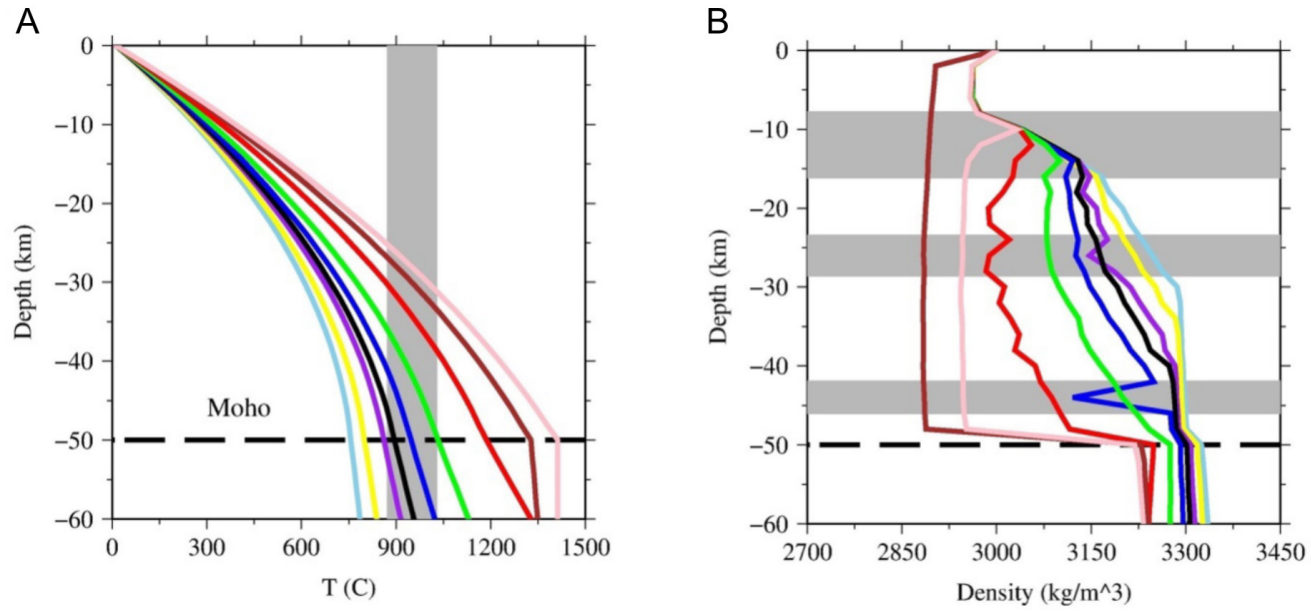


Figure 10: [A] Different geotherms of the crust. The grey zone shows the temperature band at which density reduction at ~45 km depth takes place. [B] Density profiles of the basalt corresponding to the assumed geotherms in [A]. Grey bands represent the observed reduction in density profile based on different geotherms: Pink (~15 km), red (~25 km) and blue (~45 km).

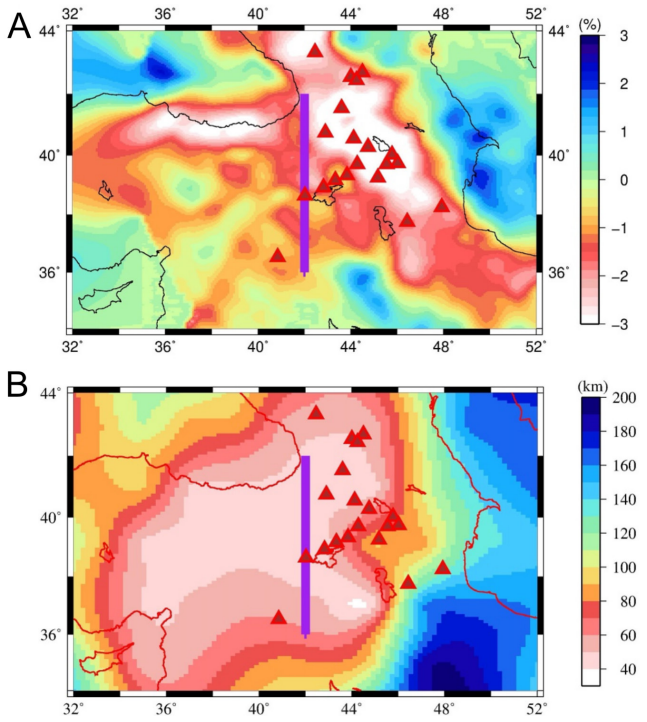


Figure 11: [A] The horizontal slice of seismic velocity Vp perturbation at depth 70 km from tomography by Koulakov [2011]. [B] LAB depth from CAM2016 [Ho et al. 2016]. Purple line depicts the location of study profile and red triangles are the location of volcanoes in East Anatolia.

relation between magma movement and thrust earthquakes, presence of strike-slip earthquakes still indicate the possible activity of the magmatic system beneath Nemrut and Suphan.

According to Julian et al. [1998], volcanic regions are expected to have strong non-double couple mechanisms. Most strike-slip solutions from full seismic moment tensor are modified after imaging the closest double couple defined from the moment tensor for earthquakes under Nemrut and Suphan (Figure 12C and 12D), while thrust events remain unchanged. The difference between focal mechanisms derived from full seismic moment tensor and the closest double couple represents the possible non-double couple component.

There are earthquakes which occur in the deep crust (30 < depth < 50 km) under Nemrut and Suphan where the temperature reaches ~ 1100 °C. This is an extraordinary observation as earthquakes (elastic release of energy) are limited to <600—700 °C at lower crustal depths. The shallow earthquakes (<30 km) occur where the temperature is less than ~700 °C. One possible explanation is that the lower crust has not molten yet, and the temperature has been increased recently. The lack of focal mechanism of deep earthquakes (>30 km) in global databases (e.g. CMT) and local studies [e.g. Bulut et al. 2012] limits comprehensive insights into the deep earthquake mechanism under Nemrut and Suphan. Therefore, the deep mechanism of earthquakes possibly caused by volume change in magma plumbing systems remains to be discovered.

## 6 Conclusions

This study presents the physical properties (temperature, density, and velocity) of the crust and upper mantle in East Anatolia, adding further constraints on the melting system, evolution, and dynamics (which can be associated with eruption and seismic activity) of the Nemrut and Suphan volcanoes. In order to achieve the above-mentioned goals, the crustal and upper mantle thermal and compositional system (well-

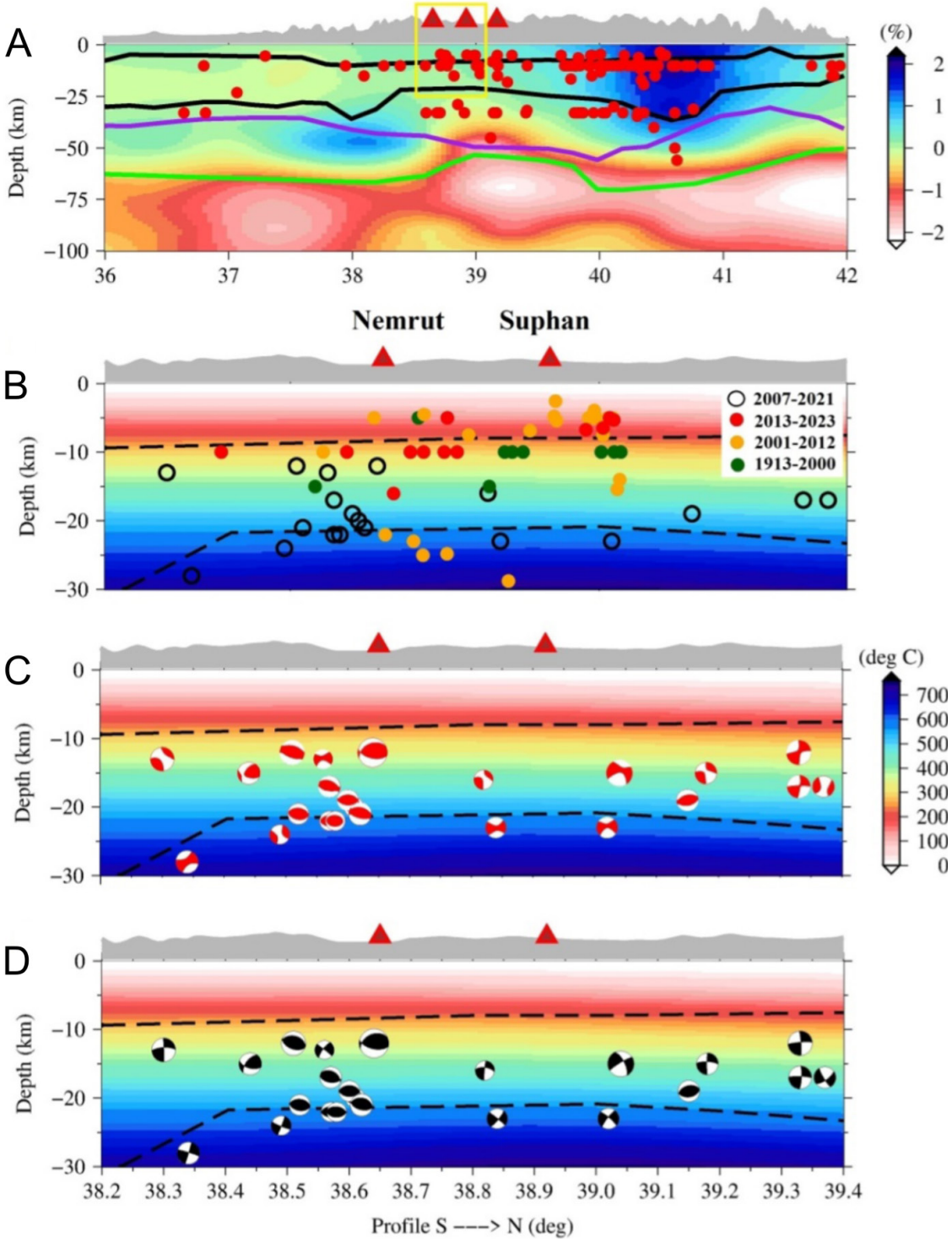


Figure 12: [A] Classification of earthquakes, volcanism, basalt assemblage, and lithospheric thinning along the study cross section. Yellow rectangle is the location of the cross section shown in [B]–[D]. [B] Temporal and spatial distributions of the earthquakes under Nemrut and Suphan volcanoes. The colored circles are earthquake depths from the USGS database (1913–2023), and empty circles are from CMT (2007–2021). [C] Focal mechanism solutions of full seismic moment tensor. [D] Focal mechanism solutions imaging possible non-double couple. Fault plane solutions are taken from the CMT program [Dziewonski et al. 1981; Ekström et al. 2012]. The color in the background of plots at [B]–[D] represents temperature.

known as thermochemical structure) is modeled using integrated geophysical-petrological approach where constraints from seismic studies (receiver functions, velocity profile, and tomography) and geochemical data on the composition of the rocks are applied. Comparison of the predicted velocity with values from independent seismological models and the fitting

of geophysical observables are used as benchmarks to accept the modeled thermochemical structure. The density change due to the thermal heterogeneities in the asthenosphere is not very big (up to 18 kg/m$^3$) at each 2-km-thick model cell in the asthenosphere. However, cumulative effects of the almost 300-km-thick column of the asthenosphere (composed of 150 vertical 2-km-thick cells), provides significant effects in the calculated gravity signal and geoid height anomaly, which is comparable with the gravity and geoid effects of the crust and the lithosphere. More importantly, geoid anomaly data is sensitive to deep parts of the model. Therefore, fitting the observed geoid height ensures the appropriateness of asthenosphere heterogeneities. Application of multiple geophysical datasets with altering depth of penetration and sensitivities to density structure ensures the accuracy of the obtained thermochemical structure.

The results of this study improve our knowledge of the magmatic system under Nemrut and Suphan. The main outcomes of this study are as follows:

1. As the temperature of the asthenosphere exceeds the solidus temperature, melting can occur at depth under Nemrut and Suphan volcanoes. The results of this study represent a warm geotherm for the crust. The obtained crustal velocity under Nemrut and Suphan is comparable with average velocity profile for volcanic areas. Regarding the absolute value of the low velocity (>4 km s$^{-1}$), there might be only a low-degree of anhydrous melting.

2. Hydrous melting is unlikely to take place in the presence of insufficient amounts of water in the asthenosphere (~100 ppm [Hua et al. 2023]). While presence of considerable amounts of melts or water reduces the density of the bulk rock, fitting geoid data suggests nearly dry asthenosphere and gravity data (Bouguer and free-air), which contradicts presence of water/melt in the crust under Nemrut and Suphan. Similarly, the derived model for crustal (chemical) heterogeneities (based on the receiver function and local geochemical data, as well as fitting geophysical data and seismic velocity profiles) suggests the presence of dry/dense basalt under these volcanoes.

3. Regarding the characteristics of the magmatic system beneath Nemrut and Suphan, the considerable lithospheric thinning correlates very well with the modeled basaltic upwelling and location of the volcanoes. Although the obtained basalt assemblage is in the solid phase, the intense seismicity and focal mechanism type (strike-slip and thrust) suggests the magma differentiations and ascent of multiple magma intrusions beneath Nemrut and Suphan. More importantly, the seismicity beneath Nemrut extends from the shallow zone to depth meaning the active magmatic system is likely fed by the asthenosphere. The presence of strike-slip and thrust earthquakes can be associated with pre-eruption magmatic activities.

4. The ongoing extension regime evidenced by different directions of plate motion (e.g. GPS velocity vectors) seemingly plays a very important role in magmatic activity in East Anatolia, while neither hydrous nor anhydrous melting seems very significant in the magma production.

5. Synthetic tests indicate that the density/velocity of the deep crust (~45 km depth) is significantly reduced when the Moho temperature is between 890—~1075 °C. The Moho temperature beneath Nemrut and Suphan exceeds ~1118 °C; so, such a reduction in physical properties is not visible. The density/velocity reduction occurs at shallower depths (~15 and ~25km depths) where the crust is warmer (~1200 and >1300 °C).

## Author Contributions

Naeim Mousavi: Conceptualization; Formal analysis; Methodology; Visualization; Roles/Writing - original draft; Writing - review and editing.

## Acknowledgements

The author is grateful to Prof. Oğuz H. Göğüş (Istanbul technical University) for his feedback and discussions. I would like to express my deep gratitude to Prof. Javier Fullea (Universidad Complutense de Madrid) for his support on the implementation of the modeling software. Sincere gratitude goes to Prof. Ling Chen (Chinese Academy of Sciences) for her constructive comments and suggestions. NM acknowledges the receipt of the PIFI grant from Chinese Academy of Sciences (CAS). This manuscript has substantially benefited from the constructive and precise comments of two anonymous reviewers. I acknowledge the edititing and comments by the editor-in-chief Prof. Jamie Farquharson. Most of the figures were produced with the GMT software [Wessel et al. 2013].

## Data Availability

Data and software used in the modeling are publicly available as referenced in the paper. Topography data (ETOPO1.0) is available in Amante [2009]. Gravity and geoid data (XGM2019) are available in Zingerle et al. [2020]. Surface heat flow is taken from Artemieva and Shulgin (2019) and Mousavi and Tatar [2024]. Earthquake hypocenters are available at United States Geological Survey [2024]. Earthquakes and plane solutions (focal mechanisms) are available at Harvard Centroid Moment Tensor catalogue (CMT). GPS velocity is taken from Reilinger et al. [2010]. Reference tomography model is taken from Koulakov [2011]. `LitMod` software for integrated geophysical-petrological modeling [Fullea et al. 2009] is open access software and is available at GitHub.

## Copyright Notice



## References

Amante, C. (2009). “ETOPO1 1 arc-minute global relief model: Procedures, data sources and analysis”. *NOAA Technical Memorandum* (NESDIS NGDC-24). [Dataset].

Angus, D. A., D. C. Wilson, E. Sandvol, and J. F. Ni (2006). "Lithospheric structure of the Arabian and Eurasian collision zone in eastern Turkey fromS-wave receiver functions". *Geophysical Journal International* 166(3), pages 1335–1346. DOI: 10.1111/j.1365-246x.2006.03070.x.

Artemieva, I. M. and A. Shulgin (2019). "Geodynamics of Anatolia: Lithosphere Thermal Structure and Thickness". *Tectonics* 38(12), pages 4465–4487. DOI: 10.1029/2019tc005594.

Artemieva, I. M. and H. Thybo (2013). "EUNAseis: A seismic model for Moho and crustal structure in Europe, Greenland, and the North Atlantic region". *Tectonophysics* 609, pages 97–153. DOI: 10.1016/j.tecto.2013.08.004.

Bartol, J. and R. Govers (2014). "A single cause for uplift of the Central and Eastern Anatolian plateau?" *Tectonophysics* 637, pages 116–136. DOI: 10.1016/j.tecto.2014.10.002.

Buket, E. and A. Temel (1998). "Major-element, trace-element, and Sr–Nd isotopic geochemistry and genesis of Varto (Muş) volcanic rocks, Eastern Turkey". *Journal of Volcanology and Geothermal Research* 85(1–4), pages 405–422. DOI: 10.1016/s0377-0273(98)00064-x.

Bulut, F., M. Bohnhoff, T. Eken, C. Janssen, T. Kılıç, and G. Dresen (2012). "The East Anatolian Fault Zone: Seismotectonic setting and spatiotemporal characteristics of seismicity based on precise earthquake locations". *Journal of Geophysical Research: Solid Earth* 117(B7). DOI: 10.1029/2011jb008966.

Cammarano, F., S. Goes, P. Vacher, and D. Giardini (2003). "Inferring upper-mantle temperatures from seismic velocities". *Physics of the Earth and Planetary Interiors* 138(3–4), pages 197–222. DOI: 10.1016/s0031-9201(03)00156-0.

Christensen, N. I. and W. D. Mooney (1995). "Seismic velocity structure and composition of the continental crust: A global view". *Journal of Geophysical Research: Solid Earth* 100(B6), pages 9761–9788. DOI: 10.1029/95jb00259.

Clark, A. N. and C. E. Lesher (2017). "Elastic properties of silicate melts: Implications for low velocity zones at the lithosphere-asthenosphere boundary". *Science Advances* 3(12). DOI: 10.1126/sciadv.1701312.

Connolly, J. (2005). "Computation of phase equilibria by linear programming: A tool for geodynamic modeling and its application to subduction zone decarbonation". *Earth and Planetary Science Letters* 236(1–2), pages 524–541. DOI: 10.1016/j.epsl.2005.04.033.

Çubukçu, H. (2008). "Petrologic evolution of Nemrut Stratovolcano (Turkiye): Peralkaline magmatism in a collisional domain". PhD thesis. Universite Blaise Pascal-Clermont Ferrand II.

Al-Damegh, K., E. Sandvol, A. Al-Lazki, and M. Barazangi (2004). "Regional seismic wave propagation (Lg and Sn) and Pn attenuation in the Arabian Plate and surrounding regions". *Geophysical Journal International* 157(2), pages 775–795. DOI: 10.1111/j.1365-246x.2004.02246.x.

Dziewonski, A. M., T.-A. Chou, and J. H. Woodhouse (1981). "Determination of earthquake source parameters from waveform data for studies of global and regional seismicity". *Journal of Geophysical Research: Solid Earth* 86(B4), pages 2825–2852. DOI: 10.1029/jb086ib04p02825.

Ekinci, Y. L., A. Büyüksaraç, Ö. Bektaş, and C. Ertekin (2020). "Geophysical Investigation of Mount Nemrut Stratovolcano (Bitlis, Eastern Turkey) Through Aeromagnetic Anomaly Analyses". *Pure and Applied Geophysics* 177(7), pages 3243–3264. DOI: 10.1007/s00024-020-02432-0.

Ekström, G., M. Nettles, and A. Dziewoński (2012). "The global CMT project 2004–2010: Centroid-moment tensors for 13,017 earthquakes". *Physics of the Earth and Planetary Interiors* 200–201, pages 1–9. DOI: 10.1016/j.pepi.2012.04.002.

Fichtner, A., E. Saygin, T. Taymaz, P. Cupillard, Y. Capdeville, and J. Trampert (2013). "The deep structure of the North Anatolian Fault Zone". *Earth and Planetary Science Letters* 373, pages 109–117. DOI: 10.1016/j.epsl.2013.04.027.

Fullea, J., J. C. Afonso, J. A. D. Connolly, M. Fernàndez, D. García-Castellanos, and H. Zeyen (2009). "LitMod3D: An interactive 3-D software to model the thermal, compositional, density, seismological, and rheological structure of the lithosphere and sublithospheric upper mantle". *Geochemistry, Geophysics, Geosystems* 10(8). DOI: 10.1029/2009gc002391.

Fullea, J., J. Rodríguez-González, M. Charco, Z. Martinec, A. Negredo, and A. Villaseñor (2015). "Perturbing effects of sub-lithospheric mass anomalies in GOCE gravity gradient and other gravity data modelling: Application to the Atlantic-Mediterranean transition zone". *International Journal of Applied Earth Observation and Geoinformation* 35, pages 54–69. DOI: 10.1016/j.jag.2014.02.003.

Goes, S., R. Govers, and P. Vacher (2000). "Shallow mantle temperatures under Europe from P and S wave tomography". *Journal of Geophysical Research: Solid Earth* 105(B5), pages 11153–11169. DOI: 10.1029/1999jb900300.

Göğüş, O. H. and R. N. Pysklywec (2008). "Mantle lithosphere delamination driving plateau uplift and synconvergent extension in eastern Anatolia". *Geology* 36(9), page 723. DOI: 10.1130/g24982a.1.

Gök, R., E. Sandvol, N. Türkelli, D. Seber, and M. Barazangi (2003). "Sn attenuation in the Anatolian and Iranian plateau and surrounding regions". *Geophysical Research Letters* 30(24). DOI: 10.1029/2003gl018020.

Griffin, W. L., S. Y. O'Reilly, J. C. Afonso, and G. C. Begg (2009). "The Composition and Evolution of Lithospheric Mantle: a Re-evaluation and its Tectonic Implications". *Journal of Petrology* 50(7), pages 1185–1204. DOI: 10.1093/petrology/egn033.

Güleç, N., D. Hilton, and H. Mutlu (2002). "Helium isotope variations in Turkey: relationship to tectonics, volcanism and recent seismic activities". *Chemical Geology* 187(1–2), pages 129–142. DOI: 10.1016/s0009-2541(02)00015-3.

Gürbüz, C. and J. R. Evans (1991). "A seismic refraction study of the western Tuz Gölü basin, central Turkey". *Geophysical Journal International* 106(1), pages 239–251. DOI: 10.1111/j.1365-246x.1991.tb04614.x.

Higgins, O. and L. Caricchi (2023). "Eruptive dynamics reflect crustal structure and mantle productivity beneath vol-

canoes". *Geology* 51(11), pages 1007–1010. DOI: 10.1130/g51355.1.

Ho, T., K. Priestley, and E. Debayle (2016). "A global horizontal shear velocity model of the upper mantle from multimode Love wave measurements". *Geophysical Journal International* 207(1), pages 542–561. DOI: 10.1093/gji/ggw292.

Holland, T. J. B. and R. Powell (1998). "An internally consistent thermodynamic data set for phases of petrological interest". *Journal of Metamorphic Geology* 16(3), pages 309–343. DOI: 10.1111/j.1525-1314.1998.00140.x.

Hua, J., K. M. Fischer, E. Gazel, E. M. Parmentier, and G. Hirth (2023). "Long-Distance Asthenospheric Transport of Plume-Influenced Mantle From Afar to Anatolia". *Geochemistry, Geophysics, Geosystems* 24(2). DOI: 10.1029/2022gc010605.

Julian, B. R., A. D. Miller, and G. R. Foulger (1998). "Non-double-couple earthquakes 1. Theory". *Reviews of Geophysics* 36(4), pages 525–549. DOI: 10.1029/98rg00716.

Kaislaniemi, L., J. van Hunen, M. Allen, and I. Neill (2014). "Sublithospheric small-scale convection—A mechanism for collision zone magmatism". *Geology* 42(4), pages 291–294. DOI: 10.1130/g35193.1.

Karabulut, H., A. Paul, T. Afacan Ergün, D. Hatzfeld, D. M. Childs, and M. Aktar (2013). "Long-wavelength undulations of the seismic Moho beneath the strongly stretched Western Anatolia". *Geophysical Journal International* 194(1), pages 450–464. DOI: 10.1093/gji/ggt100.

Karakhanian, A., R. Djrbashian, V. Trifonov, H. Philip, S. Arakelian, and A. Avagian (2002). "Holocene-historical volcanism and active faults as natural risk factors for Armenia and adjacent countries". *Journal of Volcanology and Geothermal Research* 113(1–2), pages 319–344. DOI: 10.1016/s0377-0273(01)00264-5.

Katz, R. F., M. Spiegelman, and C. H. Langmuir (2003). "A new parameterization of hydrous mantle melting". *Geochemistry, Geophysics, Geosystems* 4(9). DOI: 10.1029/2002gc000433.

Kennett, B. L. N., E. R. Engdahl, and R. Buland (1995). "Constraints on seismic velocities in the Earth from traveltimes". *Geophysical Journal International* 122(1), pages 108–124. DOI: 10.1111/j.1365-246x.1995.tb03540.x.

Keskin, M. (2003). "Magma generation by slab steepening and breakoff beneath a subduction-accretion complex: An alternative model for collision-related volcanism in Eastern Anatolia, Turkey". *Geophysical Research Letters* 30(24). DOI: 10.1029/2003gl018019.

– (2007). "Eastern Anatolia: A hotspot in a collision zone without a mantle plume". *Special Paper 430: Plates, Plumes and Planetary Processes*. Edited by G. R. Foulger and D. M. Jurdy. Geological Society of America, pages 693–722. ISBN: 9780813724300. DOI: 10.1130/2007.2430(32).

Keskin, M., J. A. Pearce, and J. Mitchell (1998). "Volcano-stratigraphy and geochemistry of collision-related volcanism on the Erzurum–Kars Plateau, northeastern Turkey". *Journal of Volcanology and Geothermal Research* 85(1–4), pages 355–404. DOI: 10.1016/s0377-0273(98)00063-8.

Koulakov, I., I. Zabelina, I. Amanatashvili, and V. Meskhia (2012). "Nature of orogenesis and volcanism in the Caucasus region based on results of regional tomography". *Solid Earth* 3(2), pages 327–337. DOI: 10.5194/se-3-327-2012.

Koulakov, I. (2011). "High-frequencyPandSvelocity anomalies in the upper mantle beneath Asia from inversion of worldwide traveltime data". *Journal of Geophysical Research* 116(B4). DOI: 10.1029/2010jb007938.

Kounoudis, R., I. D. Bastow, C. S. Ogden, S. Goes, J. Jenkins, B. Grant, and C. Braham (2020). "Seismic Tomographic Imaging of the Eastern Mediterranean Mantle: Implications for Terminal-Stage Subduction, the Uplift of Anatolia, and the Development of the North Anatolian Fault". *Geochemistry, Geophysics, Geosystems* 21(7). DOI: 10.1029/2020gc009009.

Kumar, A., M. Cacace, M. Scheck-Wenderoth, H.-J. Götze, and B. J. P. Kaus (2022). "Present-Day Upper-Mantle Architecture of the Alps: Insights From Data-Driven Dynamic Modeling". *Geophysical Research Letters* 49(18). DOI: 10.1029/2022gl099476.

Al-Lazki, A. I., E. Sandvol, D. Seber, M. Barazangi, N. Turkelli, and R. Mohamad (2004). "Pn tomographic imaging of mantle lid velocity and anisotropy at the junction of the Arabian, Eurasian and African plates: Pn tomography of the Middle East". *Geophysical Journal International* 158(3), pages 1024–1040. DOI: 10.1111/j.1365-246x.2004.02355.x.

Le Stunff, Y. and Y. Ricard (1995). "Topography and geoid due to lithospheric mass anomalies". *Geophysical Journal International* 122(3), pages 982–990. DOI: 10.1111/j.1365-246x.1995.tb06850.x.

Lei, J. and D. Zhao (2007). "Teleseismic evidence for a breakoff subducting slab under Eastern Turkey". *Earth and Planetary Science Letters* 257(1–2), pages 14–28. DOI: 10.1016/j.epsl.2007.02.011.

Mahatsente, R., G. Önal, and I. Çemen (2018). "Lithospheric structure and the isostatic state of Eastern Anatolia: Insight from gravity data modelling". *Lithosphere* 10(2), pages 279–290. DOI: 10.1130/l685.1.

McDonough, W. F. and S.-s. Sun (1995). "The composition of the Earth". *Chemical Geology* 120(3–4), pages 223–253. DOI: 10.1016/0009-2541(94)00140-4.

McKenzie, D. P. (1968). "The Influence of the Boundary Conditions and Rotation on Convection in the Earth's Mantle". *Geophysical Journal International* 15(5), pages 457–500. DOI: 10.1111/j.1365-246x.1968.tb00203.x.

– (1977). "Surface deformation, gravity anomalies and convection". *Geophysical Journal International* 48(2), pages 211–238. DOI: 10.1111/j.1365-246x.1977.tb01297.x.

Memiş, C., O. H. Göğüş, E. Ş. Uluocak, R. Pysklywec, M. Keskin, A. C. Şengör, and G. Topuz (2020). "Long Wavelength Progressive Plateau Uplift in Eastern Anatolia Since 20 Ma: Implications for the Role of Slab Peel-Back and Break-Off". *Geochemistry, Geophysics, Geosystems* 21(2). DOI: 10.1029/2019gc008726.

Molnar, P., P. C. England, and C. H. Jones (2015). "Mantle dynamics, isostasy, and the support of high terrain". *Journal of Geophysical Research: Solid Earth* 120(3), pages 1932–1957. DOI: 10.1002/2014jb011724.

Mousavi, N., V. E. Ardestani, and N. Moosavi (2022). "Slab extension and normal faulting in a low-angle subduction-related environment: An example of the Makran subduction zone (Iran-Pakistan)". *Journal of Asian Earth Sciences* 233, page 105244. DOI: 10.1016/j.jseaes.2022.105244.

Mousavi, N., J. Fullea, H. Shafaii Moghadam, and W. L. Griffin (2023a). "Mantle compositional structure and dynamics of the Arabia-Eurasia collision zone: Insights from integrated thermochemical modelling". *Gondwana Research* 118, pages 37–57. DOI: 10.1016/j.gr.2023.02.011.

Mousavi, N. and M. Tatar (2024). "Predicting heat flow in the Iranian plateau and surrounding areas based on machine learning approach". *Tectonophysics* 884, page 230403. DOI: 10.1016/j.tecto.2024.230403.

Mousavi, N., M. Tatar, H. S. Moghadam, and W. L. Griffin (2023b). "Integrated geophysical-petrological model of Damavand volcano, North Iran: Compositional structure of crust and upper mantle from seismic temperature profiling and gravity anomaly fitting". *Journal of Volcanology and Geothermal Research* 442, page 107913. DOI: 10.1016/j.jvolgeores.2023.107913.

Örgülü, G., M. Aktar, N. Türkelli, E. Sandvol, and M. Barazangi (2003). "Contribution to the seismotectonics of Eastern Turkey from moderate and small size events". *Geophysical Research Letters* 30(24). DOI: 10.1029/2003gl018258.

Özdemir, Y. and N. Güleç (2014). "Geological and Geochemical Evolution of the Quaternary Süphan Stratovolcano, Eastern Anatolia, Turkey: Evidence for the Lithosphere–Asthenosphere Interaction in Post-Collisional Volcanism". *Journal of Petrology* 55(1), pages 37–62. DOI: 10.1093/petrology/egt060.

Pearce, J., J. Bender, S. De Long, W. Kidd, P. Low, Y. Güner, F. Saroglu, Y. Yilmaz, S. Moorbath, and J. Mitchell (1990). "Genesis of collision volcanism in Eastern Anatolia, Turkey". *Journal of Volcanology and Geothermal Research* 44(1–2), pages 189–229. DOI: 10.1016/0377-0273(90)90018-b.

Pesicek, J. D. and T. Ryberg (2024). "Reference 1D Seismic Velocity Models for Volcano Monitoring and Imaging: Methods, Models, and Applications". *Seismological Research Letters* 95(5), pages 2722–2744. DOI: 10.1785/0220240070.

Portner, D. E., J. R. Delph, C. B. Biryol, S. L. Beck, G. Zandt, A. A. Özacar, E. Sandvol, and N. Türkelli (2018). "Subduction termination through progressive slab deformation across Eastern Mediterranean subduction zones from updated P-wave tomography beneath Anatolia". *Geosphere* 14(3), pages 907–925. DOI: 10.1130/ges01617.1.

Priestley, K. and D. P. McKenzie (2006). "The thermal structure of the lithosphere from shear wave velocities". *Earth and Planetary Science Letters* 244(1–2), pages 285–301. DOI: 10.1016/j.epsl.2006.01.008.

Rabayrol, F., C. J. Hart, and D. J. Thorkelson (2019). "Temporal, spatial and geochemical evolution of late Cenozoic post-subduction magmatism in central and eastern Anatolia, Turkey". *Lithos* 336–337, pages 67–96. DOI: 10.1016/j.lithos.2019.03.022.

Reid, M., J. Delph, M. Cosca, W. Schleiffarth, and G. Gençalioğlu Kuşcu (2019). "Melt equilibration depths as sensors of lithospheric thickness during Eurasia-Arabia collision and the uplift of the Anatolian Plateau". *Geology* 47(10), pages 943–947. DOI: 10.1130/g46420.1.

Reilinger, R., S. McClusky, D. Paradissis, S. Ergintav, and P. Vernant (2010). "Geodetic constraints on the tectonic evolution of the Aegean region and strain accumulation along the Hellenic subduction zone". *Tectonophysics* 488(1–4), pages 22–30. DOI: 10.1016/j.tecto.2009.05.027.

Schmincke, H.-U. and M. Sumita (2014). "Impact of volcanism on the evolution of Lake Van (eastern Anatolia) III: Periodic (Nemrut) vs. episodic (Süphan) explosive eruptions and climate forcing reflected in a tephra gap between ca. 14ka and ca. 30ka". *Journal of Volcanology and Geothermal Research* 285, pages 195–213. DOI: 10.1016/j.jvolgeores.2014.08.015.

Schutt, D. L., A. R. Lowry, and J. S. Buehler (2018). "Moho temperature and mobility of lower crust in the western United States". *Geology* 46(3), pages 219–222. DOI: 10.1130/g39507.1.

Şengör, A. M. C., S. Özeren, T. Genç, and E. Zor (2003). "East Anatolian high plateau as a mantle-supported, north-south shortened domal structure". *Geophysical Research Letters* 30(24). DOI: 10.1029/2003gl017858.

Şengül Uluocak, E., O. H. Göğüş, R. N. Pysklywec, and B. Chen (2021). "Geodynamics of East Anatolia-Caucasus Domain: Inferences From 3D Thermo-Mechanical Models, Residual Topography, and Admittance Function Analyses". *Tectonics* 40(12). DOI: 10.1029/2021tc007031.

Shaw, C. S. J., B. S. Lebert, and A. B. Woodland (2018). "Thermodynamic Modelling of Mantle–Melt Interaction Evidenced by Veined Wehrlite Xenoliths from the Rockeskyllerkopf Volcanic Complex, West Eifel Volcanic Field, Germany". *Journal of Petrology* 59(1), pages 59–86. DOI: 10.1093/petrology/egy018.

Skobeltsyn, G., R. Mellors, R. Gök, N. Türkelli, G. Yetirmishli, and E. Sandvol (2014). "Upper mantleSwave velocity structure of the East Anatolian-Caucasus region: S wave structure of Anatolia-Caucasus". *Tectonics* 33(3), pages 207–221. DOI: 10.1002/2013tc003334.

Terakawa, T., A. Kato, Y. Yamanaka, Y. Maeda, S. Horikawa, K. Matsuhiro, and T. Okuda (2016). "Monitoring eruption activity using temporal stress changes at Mount Ontake volcano". *Nature Communications* 7(1). DOI: 10.1038/ncomms10797.

Turcotte, D. and G. Schubert (2002). *Geodynamics*. 2nd edition. Cambridge University Press. ISBN: 9780521186230. DOI: 10.1017/CBO9780511807442.

Ulusoy, İ. (2008). "Etude volcano-structurale du volcan Nemrut (Anatolie de l'Est, Turquie) et risques naturels associés". PhD thesis. Université Blaise Pascal-Clermont-Ferrand II.

Ulusoy, İ., H. E. Çubukçu, E. Aydar, P. Labazuy, O. Ersoy, E. Şen, and A. Gourgaud (2012). "Volcanological evolution and caldera forming eruptions of Mt. Nemrut (Eastern Turkey)". *Journal of Volcanology and Geothermal Research* 245–246, pages 21–39. DOI: 10.1016/j.jvolgeores.2012.06.031.

United States Geological Survey (2024). *Earthquake Lists, Maps, and Statistics*. URL: https://www.usgs.gov/

natural-hazards/earthquake-hazards/lists-maps-and-statistics (visited on 01/15/2024).

Vanacore, E., T. Taymaz, and E. Saygin (2013). "Moho structure of the Anatolian Plate from receiver function analysis". *Geophysical Journal International* 193(1), pages 329–337. DOI: 10.1093/gji/ggs107.

Wessel, P., W. H. F. Smith, R. Scharroo, J. Luis, and F. Wobbe (2013). "Generic Mapping Tools: Improved Version Released". *Eos, Transactions American Geophysical Union* 94(45), pages 409–410. DOI: 10.1002/2013eo450001.

Yılmaz, Y., Y. Güner, and F. Şaroğlu (1998). "Geology of the quaternary volcanic centres of the east Anatolia". *Journal of Volcanology and Geothermal Research* 85(1–4), pages 173–210. DOI: 10.1016/s0377-0273(98)00055-9.

Zhu, H. (2018). "High Vp/Vs ratio in the crust and uppermost mantle beneath volcanoes in the Central and Eastern Anatolia". *Geophysical Journal International* 214(3), pages 2151–2163. DOI: 10.1093/gji/ggy253.

Zingerle, P., R. Pail, T. Gruber, and X. Oikonomidou (2020). "The combined global gravity field model XGM2019e". *Journal of Geodesy* 94(7). DOI: 10.1007/s00190-020-01398-0.

Zobin, V. M. (1972). "Focal mechanism of volcanic earthquakes". *Bulletin Volcanologique* 36(4), pages 561–571. DOI: 10.1007/bf02599824.